Neural Control and Modulation of Swimming Speed in the Larval Zebrafish

Neural control and modulation of swimming speed in the larval zebrafish.
Running title: Modulation of swimming speed in larval zebrafish.

Kristen E. Severi[† 1,2], Ruben Portugues[† 1*], João C. Marques[3], Donald M. O'Malley[2], Michael B. Orger[3], and Florian Engert[1*]

[†]these authors contributed equally to this work

[1]Harvard University, Department of Molecular and Cellular Biology, 16 Divinity Avenue, Cambridge MA, 02138, USA.

[2]Northeastern University Department of Biology, 360 Huntington Ave. Boston, MA, 02115, USA.

[3]Champalimaud Neuroscience Programme, Champalimaud Centre for the Unknown, Doca de Pedrouços, 1400-038 Lisboa, Portugal.

*Correspondence: rportugues@neuro.mpg.de or florian@mcb.harvard.edu

KES present address: Equipe Claire Wyart, Centre de Recherche de l'Institut du Cerveau et de la Moelle Epinier, Fondation ICM, Campus Hopitalier Pitie Salpetriere, Paris, France.

RP present address: Max Planck Institute of Neurobiology, Am Klopferspitz 18, Martinsried 82152, Germany.

Summary

Vertebrate locomotion at different speeds is driven by descending excitatory connections to central pattern generators in the spinal cord. To investigate how these inputs determine locomotor kinematics, we used whole-field visual motion to drive zebrafish to swim at different speeds. Larvae match the stimulus speed by utilizing more locomotor events, or modifying kinematic parameters such as the duration and speed of swimming bouts, the tail-beat frequency, and choice of gait. We used laser ablations, electrical stimulation, and activity recordings in descending neurons of the nucleus of the medial longitudinal fasciculus (nMLF) to dissect their contribution to controlling forward movement. We found that the activity of single identified neurons within the nMLF is correlated with locomotor kinematics, and modulates both the duration and oscillation frequency of tail movements. By identifying the contribution of individual supraspinal circuit elements to locomotion kinematics we build a better understanding of how the brain controls movement.

Highlights

- Larval zebrafish can adjust their swimming speed to match a visual stimulus.
- Ablation or activation of the nMLF implicates it in controlling swimming speed.
- Activity in identified nMLF neurons correlates with specific behavioral parameters.
- This suggests the nMLF modulates swimming by differentially driving spinal circuits.

Introduction

An important role of the nervous system is the control of locomotion in order to successfully navigate the environment. In the vertebrate brain and spinal cord, this complex task requires the selection of appropriate motor microcircuits to match the demands of any given situation, resulting in smooth and efficient movement. Critical

subcortical pathways for the initiation and control of locomotion via the basal ganglia are conserved throughout the vertebrate lineage both anatomically and functionally (Grillner et al., 2013). These regions are linked to form a control pathway in the brain with output in the spinal cord where locomotor central pattern generators (CPGs) reside. One such motor structure is the mesencephalic locomotor region (MLR), an area where electrical stimulation can initiate locomotion, as first demonstrated in cats nearly 50 years ago, and which functions across locomotor modalities, including walking, flying, and swimming (Cabelguen JM, 2003; Kashin SM, 1974; Shik ML, 1966; Steeves, 1986). From this region, signals are conveyed to glutamatergic reticulospinal cells located in the mid and hindbrain. These reticulospinal neurons are strategically located in the pathway, where visual, postural, and other sensory inputs important for selection of appropriate motor programs are thought to converge (Haehnel et al., 2012; Kohashi and Oda, 2008; Sato et al., 2007). Reticulospinal neurons excite spinal CPGs (Buchanan and Grillner, 1987; Deliagina et al., 2002; Jordan, 1998) by activating NMDA receptors essential to initiate rhythmic locomotion (Hagglund et al., 2010; McDearmid and Drapeau, 2006; Roberts et al., 2008). This sequence of activation comprises the control or descending pathway for locomotion.

An important question is how neurons in the descending pathway generate commands that produce different speeds of locomotion and how these commands are modulated by relevant sensory inputs. To investigate this, we focused on the reticulospinal step in the pathway, which serves as the conduit between the brain and the spinal cord at a critical junction for sensory-motor integration. In the larval zebrafish, the reticulospinal population consists of around 300 neurons, many of which are individually identifiable (Kimmel et al., 1982). The entire population is optically accessible, and their activity has been linked with locomotion in response to a variety of sensory stimuli (Huang et al., 2013; Kimura et al., 2013; Koyama et al., 2011).

One of these innate sensory-driven locomotor behaviors is the optomotor response (OMR) (Bilotta, 2000; Neuhauss et al., 1999) in which larvae respond to whole-field visual motion (Maaswinkel and Li, 2003; Orger et al., 2000) by swimming and turning to maintain a stable position with respect to their visual environment (Portugues and Engert, 2009, 2011). In a survey of reticulospinal activity in response to visual stimuli driving the OMR (Orger et al., 2008), the most prominent group activated by visual stimulation that specifically elicits forward-directed locomotion was found in the nMLF (nucleus of the medial longitudinal fasciculus), a cluster of reticulospinal cells in the midbrain which extends dendrites toward retino-recipient areas, and projects its axons to the spinal cord ((Gahtan et al., 2005; Kimmel et al., 1982) Wang and McLean, co-submission). This structure is known to be multi-modal and is active in response to a variety of stimuli as well as during spontaneous swimming, and is further believed to be implicated in a broad range of intensities of locomotion (Sankrithi and O'Malley, 2010).

In this study we aim to characterize the different kinematic parameters that are dynamically modulated during swimming at different speeds. Larval swimming occurs in units called bouts, where each individual bout is characterized by a discrete number of tail oscillations that propels the larva through the water. We show that different speeds of locomotion are accomplished not only by changing the speed of these oscillations, but through a dynamic interplay between the locomotor gait, and the duration, intensity,

and rate of movement episodes. The quantitative description of the behavioral output gives us a starting point to step backward through the circuit and ask how the upstream activity in the reticulospinal cells, specifically the nMLF, relates to these kinematic parameters and contributes to this modulation. We observe correlations between activity in identified nMLF neurons and both the visual stimulus, and the specific behavioral elements we identify as signatures of changing locomotor speed. We use stimulation and ablation of these cells to assess their necessity and sufficiency in modulating the various behavioral parameters. By utilizing *in vivo* two-photon calcium imaging in an awake, behaving, minimally invasive preparation, we present evidence for selective locomotor modulation by identified neurons. This study allows us to dissect the nature of activity in descending inputs that are important in controlling the speed of locomotion in an intact behaving animal.

Results

Modulation of locomotor activity in response to whole-field visual motion

In response to optomotor gratings moving at speeds from 0 to 40 mm/s, larval zebrafish adjust their locomotor speed to maintain their position relative to the moving grating. Relevant kinematic parameters were measured in an effort to quantitatively describe the behavioral response of swimming larvae. Freely swimming six day post-fertilization (dpf) wild-type larvae were individually presented with moving sinusoidal striped patterns from below, while high-speed video was acquired (Figure 1A). Analysis of the raw video (Figure 1B and Experimental procedures) allowed us to calculate relevant kinematic variables as the larva swam in response to drifting gratings moving at different speeds (Figure 1C-I). We first confirmed that larvae increase their average swim speed as grating speed increases (Figure 1C-D). Interestingly, over the course of a trial lasting several seconds (Figure 1C), they were able to match grating speeds up to 20 mm/s but their speed plateaus at 25 mm/s for gratings moving at faster velocities (Figure 1D).

Larval swimming is intermittent in what has been described previously as a beat and glide mode. This includes a “bout” period when active swimming is performed and the tail is oscillating, followed by an “interbout” period of varying duration when the larva is not actively swimming but is either coasting or stationary. A close look at the instantaneous swimming speed (Figure 1C) revealed the cyclic nature of the intermittent swimming style in the peaks and troughs of each line.

We next analyzed individual bouts and interbouts and their role in determining average swimming speed. We observed an increase in average distance per bout with grating speed (Figure 1E). Some of this could be accounted for by the lengthening of bout duration as grating speed increased within the range 0-10 mm/s (Figure 1F) whereas the increase beyond 10 mm/s is accompanied by a rise in the average tail-beat frequency (TBF) which was only modulated for bouts elicited by a grating moving faster than 10 mm/s (Figure 1G). A faster grating led larvae not only to modulate their swim bouts, but to elicit them more often: an interbout duration of 1 s for a stationary grating quickly decreased to 200 ms by the time the grating moved faster than 10 mm/s (Figure 1H). The latency of the motor response from the initiation of the grating motion was also

modulated by grating speed (Figure 1I). We saw a significant decline in latency as the speed of the grating increased, indicating that larvae initiated a locomotor response more quickly the faster the gratings were moving.

From these data we can identify relevant kinematic variables that are dynamically changing in freely swimming larvae over the range of grating speeds tested. Changes in bout duration, interbout duration, and latency appear to contribute at slower speeds, while changes in TBF are the major contributor at faster speeds. Despite this variety of factors that determine swimming speed, the larva is able to maintain a tight correlation of its own swimming speed with that of moving gratings up to 20 mm/s.

Larval swim bouts cluster into a fast and a slow type

Having determined that larvae swim faster when presented with faster OMR stimuli, we wanted to know whether they do so by continuously modulating a single type of bout or whether, as for many vertebrates, they are able to engage distinct gaits to locomote at different speeds. In the first scenario, we expect bouts to be distributed continuously throughout parameter space. Alternatively, if locomotor output is organized discretely and different types of bout are recruited, we expect the kinematic parameters across the entire bout population to cluster into two or more distinct groups.

For slow stimuli trials, the bouts formed a single cluster in a space defined by head yaw, mean TBF, rostral bend amplitude, and maximum TBF (Figure 2A, Figure S1). As the grating speed increased the original cluster shifts progressively in this space indicating a modulation of the slow swim bout, and in addition a second cluster emerged such that for fast-moving grating trials two distinct distributions with minimal overlap were observed (Figure 2B). Based on these clusters, we categorized each bout as either a slow bout or a fast bout (Experimental Procedures). We plotted the density of bouts in parameter space defined by selected kinematic variables as quantified in our assay (Figure 2C, Figure S2). To assess the consistency of the categorization we used four different kinematic parameters and found agreement in all cases (Figure 2D). The fraction of fast bouts elicited by a drifting grating changes continuously from ~4% for slow moving stimuli, to ~50% for stimuli moving at 20 mm/s or faster.

To test whether the kinematic parameters of these two different types of bouts vary with stimulus speed we repeated the analysis of Figure 1 for slow and fast bouts respectively (Movie S1). Both bout types showed a progressive modulation of speed and distance (Figure 2E, G), in response to different grating speeds, although slow bouts plateaued at just under 20 mm/s bout speed and 4 mm bout distance. Note that the fraction of fast bouts elicited was low at slow grating speeds (fewer than 10% of bouts are fast under 10 mm/s grating speed, Figure 2D). Mean TBF and maximum TBF (Figure 2H, I) were relatively constant for slow bouts, but were strongly modulated with grating speed for fast bouts. The opposite was true of bout duration (Fig. 2F), which was modulated mostly for slow bouts, and only at slow grating speeds up to around 10 mm/s, but was nearly constant for fast bouts. In summary, during slow bouts, larvae performed different numbers of oscillatory cycles at the same TBF resulting in longer bouts, whereas for fast bouts larvae swam with different TBFs over a fixed duration.

These results allowed us to quantitatively analyze the locomotor response of

larvae when presented with moving gratings at various speeds. In response to slow grating speeds larvae performed slow bouts. As the grating speed increased from 0 to 10 mm/s, the duration of these bouts increased as did their speed, resulting in bouts that spanned a greater distance, and the interbout interval was reduced. When grating speeds reached 10 mm/s, the rate and performance of slow bouts saturated and larvae began recruiting fast bouts. As the stimulus speed increased from 10 to 40 mm/s, these fast bouts were recruited more frequently. Their speed and TBF increased with grating speed resulting in more vigorous bouts.

When presented with a whole-field moving visual stimulus, did larvae measure their speed and then recruit the appropriate locomotor output, or did they start with a slow bout and then recruit faster bouts if the outcome of the previous motor output was insufficient? Was there an order in the recruitment of bout type and how did this order depend on the speed of the grating? To answer these questions, we computed the probability of a bout being slow or fast according to its position in the sequence of bouts for a trial with a given stimulus speed (Figure 2J). In fast trials, larvae often began with slow bouts and the probability of using fast bouts increased throughout the trial. This phenomenon was consistent with behavioral responses in a motor learning assay using an OMR stimulus in head-embedded larvae, where larvae were able to adjust their motor output if it did not match their expectation (Ahrens et al., 2012; Portugues and Engert, 2011). These different types of bouts were recruited as needed with variation of kinematic parameters, namely the bout duration, and TBF, determining the swimming speed. In the following experiments we ask questions regarding the modulation of these variables by descending motor control neurons.

Restrained larvae also perform the OMR but only utilize slow bouts

With a view to monitoring neural activity in a restrained or paralyzed larva we characterized the changes in kinematic variables in head-restrained larvae, in an arrangement where the head remained stationary in agarose but the tail was free to move. In this restrained preparation, larvae were still able to reliably perform the OMR by moving their tail in response to drifting gratings. Larvae viewing drifting gratings in this open-loop configuration increased the duration of bouts (Figure 3A), and decreased both the interbout duration (Figure 3B) and the latency to initiate swimming (Figure 3C) with increasing grating speed, consistent with the behavior of freely swimming larvae. These parameters, along with TBF, were the focus of our analysis since other parameters investigated in Figures 1 and 2 are not relevant in head-restrained larvae.

In order to identify what types of bouts larvae were performing in the head-restrained preparation we compared the distribution of elicited bouts by maximum TBF to that obtained in the freely swimming experiments reported in Figures 1 and 2, where larvae perform both slow and fast bouts. We used maximum TBF as a kinematic parameter because we expected it to be least disrupted by the restrained preparation. For restrained larvae (Figure 3D, black), bouts most often contained a maximum TBF around 30 Hz, even at fast grating speeds. The shape of these distributions matches that observed in freely swimming larvae (Figure 3D, gray) for slow speeds but differs significantly at fast grating speeds (30 mm/s). At fast speeds, freely swimming larvae

executed bouts that contain maximum tail-beat frequencies often exceeding 65 Hz, which was rarely observed in restrained larvae. These frequencies are those associated with fast bouts, from which we conclude that in the restrained preparation larvae robustly perform the OMR to gratings moving at different speeds, but rather than utilizing fast bouts they do so mainly by modulation of slow forward bouts, evident by the shift in maximum TBFs from slow to medium TBFs, but never to fast TBFs. Therefore we focus on the modulation of the speed of slow bouts, which we consider to be kinematically similar to the “slow swim” gait described previously (Budick and O'Malley, 2000) in the restrained preparation. These behavioral experiments provided an essential starting point from which to investigate the neural control of this motor behavior. The delicate adjustment of kinematic variables resulted in the larva responding to a faster grating with motor output which enables covering a greater distance over time.

Laser ablation of nMLF cells reduces maximum swimming speed in response to drifting gratings

The next question we asked was whether removal of descending neurons would affect swimming speeds, thus implicating them in speed modulation. Following previously described methods (Huang et al., 2013; Orger et al., 2008) we used two-photon laser ablation of bilaterally–symmetrical individual neurons to test the effect on optomotor swimming behavior in response to various speeds of visual gratings (Experimental Procedures). The nMLF is a nucleus located in the midbrain consisting of ~20 neurons on each side (Figure 4A, Movie S2). In light of previous work describing activity of different reticulospinal cell populations in response to presentations of moving gratings (Orger et al., 2008), we hypothesized that the nMLF was a strong candidate for controlling forward optomotor swimming, since it showed bilaterally symmetric visual responses, whose direction tuning matched the behavioral tuning of forward swims. We targeted three groups within the reticulospinal neurons for laser ablation: large cells of the nMLF, cells in the RoM cluster, and the Mauthner cells (Figure 4A). Eight of the nMLF neurons, which are larger in size than the others, are named MeLr, MeLc, MeLm and MeM, with one of each type in each half of the brain (Kimmel et al., 1982). We always ablated at least 4 of these 8 neurons, a small subset of the nMLF by number, but the only individually identifiable cells between larvae. We suspected that ablating fewer would result in imperceptible phenotypes. In control regions, 4-8 RoM neurons were ablated per larva, or alternatively both Mauthner cells were ablated. We recorded the behavioral response to several grating speeds using high-speed video before and after laser ablation of targeted cells (Figure 4B). Behavioral responses in RoM-ablated larvae and Mauthner-cell ablated larvae were similar and are pooled below for simplicity. Compared with pre-ablation larvae, only the nMLF-ablated larvae showed a consistent and significant deficit in achieving high speeds of swimming in response to visual stimuli (Figure 4C-D, Figure S3). This finding applied to all of the parameters we recorded, including bout duration, maximum TBF, bout distance, and bout speed, indicating a general deficit in modulation of swimming speed in response to a large range of grating speeds as compared to controls which showed no deficit.

Strength of stimulation of the nMLF is correlated with aspects of elicited swimming

We next asked whether activation of the nMLF produced a locomotor response. We developed a protocol for direct electrical microstimulation of the nMLF to establish the sufficiency of nMLF activity for generating swimming behavior. When electrical pulses of a given intensity and frequency were delivered to the midbrain (Experimental Procedures), the larva responded with distinct locomotor patterns (Figure 5A). The tail underwent rhythmic undulation in a consistent and smooth way, and there was little movement outside of the time period when pulses were delivered. The cyclic nature, TBF and maximum bend position along the tail indicate these movements were not struggle or escape responses, which were mostly avoided by careful selection of stimulation parameters. The nMLF cells were activated during this induced locomotion, verified by calcium imaging using calcium green dextran (Figure 5B). These data were collected from non-paralyzed larvae, so calcium imaging trials could be interleaved with high-speed behavioral movies in the same larva. We observed consistent activation concurrent with the start of each pulse train, and calcium indicator fluorescence rose over the course of the train delivery.

We modified the stimulation parameters by increasing both the current and the frequency of the pulses delivered. Whereas increasing the current had no significant effect (data not shown) increasing the pulse frequency resulted in an increase in bout duration (Figure 5C) and an increase in maximum TBF (Figure 5D). These results suggested that the stimulated neurons were activated more strongly under these higher frequency conditions. We confirmed this by measuring the maximum $\Delta f/f$ of the calcium response in all cells across all larvae in response to the varying stimulation parameters, and concluded that the frequency of stimulation modified the amplitude of the calcium response in large nMLF neurons (Figure 5E). It is worth noting that the kinematic values for the data in Figure 5 have a similar range to the data in freely swimming and restrained larvae swimming in response to drifting gratings (Figures 1,3).

To confirm that these behavioral and calcium effects were dependent on stimulation of a specific region containing the nMLF, we used the minimum threshold for activation and moved the stimulation pipette incrementally away from its initial position adjacent to the nMLF somas, while testing behavioral and nMLF responses at each position (Figure S4). We observed a response in >95% of trials with the pipette position less than 60 μm away from the cell borders, and in <5% of trials at distances greater than 60 μm. We observed in all larvae (n = 10) that failure to elicit a behavioral response always correlated with failure to elicit a calcium response. Interestingly, we always observed either bilateral activation of the entire nucleus across both sides of the midline or no activity at all. These data indicated that electrical stimulation of the nMLF was sufficient to elicit swimming, and that the stimulation parameters which modified aspects of the locomotor output, namely bout duration and TBF, also modified activity in the nMLF.

Population activity in the nMLF as grating speed varies

We next investigated the activity of the population of nMLF neurons during presentations of gratings of different speeds. Are there a greater number of nMLF

neurons recruited as grating speed increases, or do activity patterns of nMLF neurons vary with grating speed? To address these questions, we utilized *in vivo* two-photon calcium imaging of nMLF neurons loaded with calcium green dextran in paralyzed larvae presented with drifting gratings moving at one of five speeds (Figure 6A). By retrogradely labeling a large subset of the population, we were able to monitor the population as a whole, including the eight individually identifiable large cells (MeLr, MeLc, MeLm, and MeM in both the left and right clusters) and small cells in the left and right clusters (Figure 6B). An example of calcium responses of three cells to these different stimuli is shown in Figure 6C. These calcium responses were consistent with targeted cell-attached electrophysiological recordings from large nMLF neurons (Figure S5). We observed no lateralized differences in responses so examples from the left and right sides of the midline were pooled for further analysis. Analyzing these calcium responses as a function of grating speed revealed interesting differences. The maximum Δf/f of the calcium response changed across speeds (Figure 6D) and did so differently for the large and small cells: small cell responses appeared to be more uniform across speeds and their latency was found to decreases slightly less as grating speed increases (Figure 6E). We observed a marked difference between the MeM cells and the other three types of large nMLF cells, the MeL cells. MeM cells showed a significant decrease in activity for the fastest moving grating speed and the latency to peak signal was two seconds longer across all speeds.

Monitoring neural activity using calcium imaging allowed us to investigate whether recruitment of neurons to the active pool was growing as grating speed increased. We plotted the fraction of cells that were active when presented with the various speed of moving grating (Figure 6F) and found large cells were active 100% of the time. However, only a fraction of small cells responded but this fraction remained constant at around 80% across grating speeds. We concluded from these results that no recruitment of nMLF cells was occurring as the grating speed increased. This suggested that if the nMLF was involved in behavioral modifications with increasing speed, as was indicated by the results presented previously, this occurred as a result of the change in activity of already active cells rather than the recruitment of previously inactive cells. We found the largest modulation of activity in the large cells that we focused on the in following experiments.

Correlation of nMLF calcium activity with both sensory input and motor output in restrained, actively swimming larvae

To clarify the role of individual nMLF neurons in modulating the various swimming parameters, we monitored their activity using two-photon calcium imaging in the head-restrained preparation (Figure 7A, Movie S3). This made it possible to correlate neuronal activity with both sensory input (grating motion) and restrained active swimming with minimal motion artifacts that can be corrected for (Experimental procedures and Figure S6). It should be noted that calcium signals persist when the larva is paralyzed and motor output is recorded using fictive ventral root recordings (Figure S7). A portion of a representative experiment is shown in Figure 7B. The experimental protocol involved alternating 10 s periods of a static grating with forward

grating motion at different speeds (5, 10 and 30 mm/s shown at the top). In these experiments larvae performed the majority of swim events while presented with the two slower moving gratings (Figure 7C). We imaged the nMLF, which had previously been labeled with calcium green dextran and presented the visual stimuli in each imaging plane (80 planes, 1 μm between planes, Experimental Procedures and Supplementary Materials). The fluorescence traces of six cells recorded simultaneously are shown in blue. We monitored tail motion using a high-speed camera and the cumulative angle along the tail is shown in black at the bottom (higher temporal resolution behavior is shown in Figure 7D). In this way we aimed to correlate the activity of individually identified neurons with specific behavioral parameters from individual bout events recorded simultaneously.

We first asked whether the activity of the four types of large nMLF cells correlates best with sensory input or with motor output (Figure 7E). We averaged the fluorescence for each of the four large nMLF cells over all stimulus presentations for the three grating speeds presented (to calculate the sensory-triggered activity), and separated these into presentations during which the larva executed bouts (Figure 7E, top row) and those which did not elicit swimming (Figure 7E, middle row). We found that nMLF cells were only active in presentations during which bouts occurred. This activity was greater for grating speeds of 5 and 10 mm/s. When presented with a forward moving grating, larvae typically performed a forward swim bout such as in Figure 7D. Rarely, larvae performed other behavioral maneuvers (Figure S8).

We subsequently aligned the calcium activity of each cell based on the timing of bout events to find the motor-triggered response of the four large nMLF cell types (Figure 7E, bottom row). The motor-triggered responses were similar across speeds. We concluded from these results that activity in the nMLF was motor related, and that the larger sensory-triggered activity at 5 and 10 mm/s grating speed is solely a result of the fact that these speeds elicit more bouts (Figure 7C). We observed that the responses measured in MeMs were generally smaller than those measured in the MeLs. The results in Figure 7E suggest nMLF activity in response to optomotor gratings is not sensory related but is rather locked to the timing of swim bouts.

We analyzed the correlation of nMLF activity with the individual kinematic parameters of forward swimming, and used the bout duration and the maximum TBF to represent bout intensity. When each bout was performed we measured the maximum $\Delta f/f$ in a short window encompassing the bout. We used this maximum $\Delta f/f$ as a measure of the neuronal activity and correlated it with the kinematic parameters of each bout (Figure 7F-G). For each cell in each larva a linear regression was performed between the neuronal activity and the kinematic variable. Figure 7F shows the analysis for a representative larva, where neuronal activity was regressed against bout duration. Activity in MeLr and MeLc correlates significantly with bout duration, whereas that of MeLm and MeM does not (method of determining significance in Figure S9). Across all larvae, we found that 82% (31/38) of MeLr cells had activity which correlated significantly with bout duration (Figure 7H), suggesting a role of this cell type in the control of this behavioral variable. Neuronal activity was also regressed against maximum TBF (example larva shown in Figure 7G, where both MeLr and MeLc show a

significant correlation). We found that activity in 89% (16/18) of MeLc cells showed a significant correlation with maximum TBF (Figure 7I).

From these experiments including imaging of neuronal activity, behavioral monitoring, and correlation of the former to different features of the latter, we learned that the nMLF is active when larvae perform swim bouts. Furthermore, we concluded that activity in all four types of large nMLF cell was related to motor output but differently so. The activity in MeLr and MeLc correlated well with bout duration and maximum TBF respectively, kinematic parameters consistent with the ablation and stimulation experiments presented earlier (Figures 4-5). These findings reinforce the importance of anatomically mapping and functionally connecting the specific roles these large nMLF neurons play with their downstream targets in the spinal cord, a topic addressed in Wang and McLean (co-submission).

Discussion

The OMR in larval zebrafish is comprised of orientation and locomotor movements in response to whole-field visual motion patterns and has been widely studied in the context of large-scale forward genetic screens for visuo-motor defects (Muto et al., 2005; Neuhauss et al., 1999), and psychophysical and physiological characterization of vision (Maaswinkel and Li, 2003; Orger et al., 2000). In this study we conducted a detailed quantitative description of locomotor behavior to dissect the variation and modulation of swimming in response to varying a single parameter of the visual stimulus: speed. This allowed us to better define the OMR as a visuomotor transformation from whole-field visual motion of different speeds to locomotor behavior. To better understand how the brain controls this visuomotor behavior, we investigated the nMLF, a multifunctional descending motor nucleus that is involved in a variety of behavioral contexts (Gahtan et al., 2005; Orger et al., 2008; Sankrithi and O'Malley, 2010). Electrical stimulation and laser ablation of the nMLF suggested its participation in dynamically executing differential motor output required to achieve different speeds of swimming. When we performed functional calcium imaging in restrained, behaving larvae, we found that activity of the nMLF, and in particular two identifiable cells: MeLr and MeLc, is correlated with specific kinematic aspects of swimming: the bout duration and the maximum TBF.

For visual motion slower than 10 mm/s, larvae swim using mostly slow bouts. The kinematic parameters of these bouts are similar to the “slow swim maneuver” (Budick and O'Malley, 2000) which constitutes a locomotor gait based on axial movement in conjunction with an alternating pectoral fin pattern (Green et al., 2011). We observe both these motifs in the midbrain electrical stimulation preparation when the fins are not enclosed in agarose (data not shown). Eliciting bouts more frequently and increasing their duration and intensity would permit modulation of this baseline motor pattern without changing the main components of the gait, which is consistent with our observations. When the speed of the visual motion exceeds 10 mm/s, larvae begin recruiting a considerable proportion of fast bouts. The responses to fast moving gratings have values which resemble the kinematic features that describe “burst swimming”, a distinct gait primarily associated with the escape response (Budick and O'Malley, 2000).

The OMR is generally considered to be a routine navigational behavior, and the ethological relevance in the natural environment of visual motion at fast speeds in our assay that elicits these “burst swims” is unknown. The fact that larvae can track whole-field visual motion well up to 20mm/s suggests this is the upper limit of what they naturally encounter.

The complete circuit required to perform the OMR begins with the retina, which relays signals to the brain via the ten identified retinal ganglion cell arborization fields (Figure 8) (Burrill and Easter, 1994; Robles et al., 2011). Identifying which arborization fields are involved in the OMR, and how grating speed is encoded and transmitted to the locomotor circuitry elements such as the nMLF remains unknown. The OMR is known to persist in the absence of the optic tectum, the largest of these processing areas (Roeser and Baier, 2003), and when we imaged larvae expressing the fluorescent protein dendra under the control of a promoter that drives expression in retinal ganglion cells (atoh7/ath5) (Kay, 2001; Masai, 2003) we saw no regions of direct overlap with the reticulospinal population (Figure S10). This suggests connections are indirect and via non-tectal retino-recipient areas such as the pretectum. Recent work has identified pretectal areas in zebrafish involved in processing whole-field motion (Kubo et al., 2014; Portugues et al., 2014). The nMLF has been implicated in other behaviors heavily reliant on vision such as prey tracking and capture (Bianco et al., 2011; Borla et al., 2002; Westphal and O'Malley, 2013), since ablation of large cells impairs the ability of larvae to feed (Gahtan et al., 2005). We suggest based on the findings made here that larvae lacking proper nMLF function may lack regulation of bout duration and maximum TBF, reducing their capability to hunt.

It is interesting to consider potential inputs to the nMLF and reticulospinal cells that could be critical for sensory-motor integration. The olfactory inputs to motor control centers have been well established in the lamprey preparation from the olfactory epithelium to the reticulospinal cells, passing through the posterior tuberculum and the MLR (Figure 8) (Derjean D, 2010). This connection from the cholinergic MLR is thought to drive bilateral reticulospinal cells symmetrically and monosynaptically from the MLR on one side (Brocard et al., 2010). The MLR has yet to be conclusively identified in the zebrafish, with no unidentified midbrain clusters of cholinergic cells observed in larval immunostaining (Arenzana et al., 2005). There are other neuromodulators thought to be present in the area immediately surrounding the nMLF, with identified terminals staining positive for TH and 5-HT (McLean and Fetcho, 2004), and dopaminergic and noradrenergic tracts target the area (Tay et al., 2011), but direct connections with nMLF neurons have yet to be established. The tangential nucleus contributes to vestibular-correction of eye position by relaying information sensed by utricular otoliths in the ear to oculomotor nuclei, with axonal arbors targeting the contralateral nMLF (Figure 8) (Bianco et al., 2012). This could provide a direct pathway for vestibular information to reach locomotion control centers. With these various sensory modalities providing inputs, the reticulospinal array could serve as an integration center for sensory cues directing navigation of the environment.

The two bout types observed here in freely swimming larvae lead to an important question: how are the activity patterns required to produce these different types of bouts

produced by spinal central pattern generators? Recent work in the mammalian spinal cord revealed some of the complexity of glutamatergic inputs, showing that non-NMDA and NMDA receptor systems can function in parallel and independently to contribute to locomotor speed and stability (Talpalar and Kiehn, 2010). A new principle in spinal circuit organization has emerged in which different outputs arise from a shared pool of available neurons, through the selective recruitment of a set of multifunctional and specialized interneuron classes (Berkowitz et al., 2010). Many morphological classes of these interneurons and their genetic identities have been identified across vertebrate model organisms (Goulding, 2009; Hale et al., 2001; Roberts et al., 2010), and functional studies have revealed distinct patterns of activity across these identified interneuron types and their role in the generation of rhythmic locomotor patterns (Crone et al., 2009; Gosgnach et al., 2006; Wyart et al., 2009). In zebrafish some excitatory classes of spinal interneurons are exclusively active during fast or slow swimming (McLean et al., 2008; Ritter et al., 2001). The dorsal-ventral position of these excitatory interneurons is tightly correlated with the minimal swimming frequency at which the neuron is active (McLean et al., 2007), suggesting a utilization of a continuously varying set of interneuron cell types through smoothly graded shifts in locomotor speed. This is consistent with the idea of slower and faster swimming patterns being driven by partially overlapping CPGs, which, while allowing distinct gaits to be executed might also allow for graded changes in speed.

The implementation of bouts and interbouts is shown here to be an important way larvae modulate swimming speed, and the spinal mechanisms controlling the duration and intensity of bouts at a particular frequency are not known. In *Xenopus*, dedicated descending GABAergic “stopping” neurons (Li et al., 2003) or build-up of adenosine in the spinal cord (Dale, 2002) may contribute to bout termination. Serotonin has been shown to reduce the interbout period, resulting in increased motor output, in both active and fictive swimming (Brustein et al., 2003). New work incorporating network rhythmicity and intrinsic properties of motor neurons showed how the zebrafish can accomplish increases in swimming frequency using a specific pattern of motor neuron recruitment (Menelaou and McLean, 2012), and this pattern of segregation of motor neuron pool by swimming frequency continues to adult stages (Ampatzis et al., 2013). The behavioral observations we present here are the first case where this broad range of swimming speeds has been experimentally evoked in an intact, non-paralyzed preparation, and this experimental paradigm provides an additional tool to study these CPG mechanisms.

Studies of anatomical links between nMLF cells and the spinal cord have shown a decrease in the density of collaterals with increasing distance along the tail (Gahtan and O'Malley, 2003). This is consistent with the idea of nMLF neurons providing a tonic signal to activate rostral spinal segments which then propagate a wave of excitation caudally to generate forward motion, and the spinal circuits necessary for episode duration control were recently localized to rostral segments (Wiggin, 2012). Wang and McLean (co-submission) makes a leap forward, by mapping both anatomical and synaptic connections between identified nMLF neurons and motor neuron targets. We find their study particularly intriguing and suggestive, as they show broad outputs from

the nMLF to the spinal motor pool can be transformed into specific patterns of recruitment based on the intrinsic biophysical properties of motor neurons (Figure 8). Our observation that faster bouts elicited during the presentation of whole-field motion are associated with increased activity in the nMLF would result in greater motor neuron activity, creating more intense body bends, as we observe during the faster swimming responses to drifting gratings. Like motor neurons, excitatory spinal interneurons are also recruited in a dorso-ventral pattern depending on the intensity of locomotion (Bhatt et al., 2007; McLean et al., 2007; McLean et al., 2008). The model that arises from these studies is that neurons within the nMLF may differentially innervate the spinal networks on the basis of axonal projections, but different individual cells may have differences in their targets. Both MeLr and MeLc may project to motor neurons, but MeLr may also activate interneurons regulating bout duration, while MeLc may project to interneurons regulating TBF. Thus the nMLF could dictate not only motor neuron recruitment but also the participation of different premotor elements to coordinate appropriate responses to visual inputs.

In this study we attribute to the nMLF a major role in the control of the speed of locomotion. We believe the identification of how specific individual cells affect the behavioral parameters modulated when larvae swim at different speeds is an important step toward understanding the relationship between supraspinal control elements and locomotor output.

Experimental Procedures

Animal care

Fish were reared on a 14/10 hour light/dark cycle at 28 °C. Animal handling and experimental procedures were approved by the Harvard University Standing Committee on the Use of Animals in Research and Training (Cambridge, MA, USA), by the Champalimaud Foundation Ethics Committee and by the Portuguese Direcção Geral de Veterinária and were according to the European Directive 2010/63/EU.

Freely-swimming behavioral assay

6dpf Tubingen WT zebrafish larvae swam freely in a 150 mm x 10 mm rectangular acrylic arena with 8 mm depth containing E3 medium. Their behavior was recorded from above at 700 Hz using an IR-sensitive, high-speed camera (MC1362, Mikrotron), fitted with a machine vision lens (Schneider apo-Xenoplan 2.0/24) and a 790 nm long pass filter. Larvae were illuminated from below by a 20 x 10 cm LED backlight (850 nm, Nerlite). A sine wave grating with spatial period of 10 mm drifting at different speeds was projected onto a 150 mm x 150 mm opal glass diffuser 5 mm below the larva using a DLP projector (BenQ). Stimulus presentations were initiated when the larva remained for 5 s in one of the extremes of the arena and terminated when the larva reached the opposite end or after 30 s had elapsed. If a larva failed to reach the opposite end during this period, a 10 mm/s grating was displayed until it swam the remaining distance. Acquisition, stimulus presentation, tracking, and tail segmentation were performed online by a custom written program (Visual C#, Microsoft). The location of the larva was determined by similar methods to previous studies (Burgess and Granato, 2007). The rostral bend amplitude was measured as the maximum peak-to-peak bend amplitude 1.17 mm caudal to the swim bladder in our analysis. See Supplemental Materials.

Head-embedded behavioral assay

The behavioral assay was performed as in Portugues and Engert, 2011 with the difference that the tail was tracked with software custom written in Labview in real time at 700 Hz. 10 s trials were separated by 30 s inter-trial intervals during which the grating was static. The grating speeds (3, 5, 8, 10, 15, 20, 25, 30 and 40 mm/s) were presented 5 times in random order.

Two-photon laser ablations and testing behavior

4 dpf nacre -/- larvae were injected with texas-red dextran as described previously ((O'Malley et al., 1996; Orger et al., 2008) Supplemental Materials), and allowed to recover for 24-48 hours. Pre- and post- ablation behavior was tested individually in a 150 mm x 10 mm arena, imaged at 205 Hz with an MC1362 Mikrotron camera with IR illumination. Larvae were sequentially shown a forward grating for 10 s (moving at moving at 5, 10, 20, or 30 mm/s) during which high-speed video was acquired, a stationary grating for 10 s, followed by a grating moving at 10 mm/s in the opposite direction for 20 s to return the larva to the initial side of the arena. 5 trials of each speed were presented in random order. Following the monitoring of pre-ablation behavior, larvae were embedded in 1.2% low melting point agarose and imaged under two-photon using 910-920 nm. Reference stacks were acquired, and then 4-8 cells were ablated from either the nMLF, or a control region (RoM 2/3), or a bilateral Mauthner cell ablation. Ablations were performed as previously described (Huang et al., 2013; Orger et al., 2008) and damage was well localized to the target region (Figure S11). Following ablation, larvae were un-embedded and placed in a well with E3 medium to recover for at least one hour. Following the monitoring of post-ablation behavior, each larva was re-embedded and imaged 4-6 hours post-ablation where cell ablation was confirmed in 177/178 attempts.

Electrical stimulation

A solution containing 10% calcium green dextran (3,000 MW, Invitrogen) and 10% texas-red dextran (3,000 MW, Invitrogen) in water was pressure injected using the same method. Larvae were embedded in 2% low melting temperature agarose and the agarose surrounding the tail was removed. Glass pipettes of 33 mΩ resistance containing external solution and silver wire were connected to a SD-9 Grass stimulator. Stimulus pulses were 10 ms in duration. Five frequencies of stimulation were used (2, 4, 6, 8 and 10 pulses per second) between 0.30 and 0.60 μA and were selected in random order. Calcium responses from nMLF cells to electrical stimuli were recorded on a Hamamatsu ORCA-ER CCD camera at 20 Hz and analyzed using custom software (Labview, National Instruments and Matlab, Mathworks).

Two-photon imaging of nMLF cells in paralyzed larvae

Larval zebrafish were spinally injected with calcium green dextran at 4 dpf as above and used for experiments at 6-7 dpf. Larvae were paralyzed by immersion in 20 μl of α-bungarotoxin solution (1 mg/ml in E3 medium) until they showed no motor activity and embedded in 2% low melting point agarose on a 35 mm petri dish with a sylgard bottom filled with E3 medium. Stacks were taken of the nMLF consisting of 40 planes, each imaged for 200 s, with 2 μm separation, and a visual stimulus with 10 trials of moving gratings, each lasting 10 s, with 10 s of static gratings in between trials. Data were analyzed using software custom written in Matlab (Mathworks).

Two-photon imaging in behaving larvae

Same injection and embedding protocol as above (without paralysis) but agarose was removed to free the larva's tail. 80 planes, 1 μm apart and encompassing all the nMLF were imaged for 120 s each. A visual stimulus was shown consisting of a square wave grating of period 1 cm presented 5 mm below the larva. The stimulus alternated every 10 s between static and moving

in a caudal to rostral direction (speeds shown were 5, 10, and 30 mm/s, twice each per plane). The larva's tail was tracked online at 200 Hz using a PikeF-032B high-speed camera (AVT) and IR illumination, allowing simultaneous monitoring of behavior and neural activity. Image time series were x-y motion corrected using Matlab software (David Heeger, New York University) and analyzed with custom-written Matlab software.

Acknowledgements

The authors thank Filippo Del Bene for providing Ath5:Gal4;UAS:Dendra larvae (Arrenberg et al., 2009). KES received financial support from the Institut du Cerveau et de la Moelle épinière (ICM), the Philippe Foundation, and the European Research Council (ERC) starter grant OptoLoco. RP thanks the Human Frontier Science Program for funding through fellowship LT01115/2007-C. MBO was supported by Marie Curie Career Integration Grant PCIG09-GA-2011-294049 and by the Fundação para a Ciência e a Tecnologia (FCT), PTDC/NEU-NMC/1276/2012. JCM was supported by a PhD fellowship from the Portuguese Fundação para a Ciência e a Tecnologia. FE was supported by NIH grants DP1 NS082121 and R01DA030304. The authors thank Isaac Bianco, Adam Kampff, Kuo-Hua Huang, Tod Thiele, and Claire Wyart for useful discussions and thank David McLean for critical reading of the manuscript and valuable comments.

Figure Legends

Figure 1. Larval swimming speed depends on OMR grating speed

Relevant kinematic variables which describe larval zebrafish swimming are plotted against grating speed over a range of 0-40 mm/s. (A) Schematic of experimental design for freely-swimming larvae. High-speed video was acquired from above with drifting gratings projected on a screen below the arena, and larvae illuminated with IR light. (B) Image processing involved background subtraction and inversion, determination of the global maxima (green point), and tail curvature (Experimental Procedures, Supplemental Materials). Scale bar = 2 mm. (C) Instantaneous swimming speed vs. grating speed. Traces are aligned such that zero on the x-axis is the initiation of the first bout in the direction of the stimulus motion. For data to the right of the black line (left of this line indicates orienting maneuvers the larva uses to align its body with the axis of motion of the grating), we see the difference in swimming speed as a function of grating speed, but also the timing during which this swimming speed varies with respect to initiation of grating motion. Panels (D-I) represent data from 52,938 bouts from 45 freely swimming larvae. (D) Average swimming speed during trial (mm/s) vs. grating speed. (E) Average bout distance (mm) vs. grating speed. (F) Average bout duration (ms) vs. grating speed. (G) Average tail-beat frequency elicited during a bout (Hz) vs. grating speed. (H) Average interbout duration (ms) vs. grating speed. (I) Latency (ms) vs. grating speed. Error bars on all plots are the SEM.

Figure 2. Larvae swim by eliciting bouts that cluster into two types

(A) Bouts elicited at slow grating speeds. Joint distributions of several pairs of relevant kinematic parameters including mean tail-beat frequency, head yaw, rostral bend amplitude, maximum tail-beat frequency. (B) Distributions of the same parameters as in A for bouts elicited at fast grating speeds. Slow pool data (0, 1, 2, 3 mm/s gratings) and fast pool data (25, 30, 35, 40 mm/s gratings). Additional grating speeds plotted in Figure S1. (C) Fitting of rostral bend amplitude (upper) and head yaw (lower) parameters with binormal distributions to establish the threshold between fast and slow bouts plotted below. Additional parameters plotted in Figure S2. (D) Fraction of bouts that are fast as determined by different kinematic parameters: yaw,

rostral bend amplitude, maximum bout speed, and mean tail-beat frequency. (E) Average bout speed (mm/s) vs. grating speed for fast (red) and slow (blue) bouts. (F) Average bout duration (ms) vs. grating speed. (G) Average bout distance (mm) vs. grating speed. (H) Average tail-beat frequency (Hz) vs. grating speed. (I) Average maximum tail-beat frequency elicited during a bout (Hz) vs. grating speed. (J) Probability that a bout will be slow (blue) or fast (red) for different grating speeds plotted by the order of bouts elicited (bout number) independent of time. Error bars on all plots are the mean +/- SEM (n= 52,938 bouts from 45 larvae).

Figure 3. Restrained OMR kinematic parameters
By restraining the head in agarose but leaving the tail free to move, we extracted kinematic parameters from restrained swimming to compare with free swimming (n = 25 restrained larvae). (A) Mean bout duration (ms) vs. grating speed. (B) Interbout duration (ms) vs. grating speed. (C) Latency (ms) vs. grating speed. (D) Histograms of the number of bouts elicited by maximum tail-beat frequencies for four grating speeds: 0, 5, 10 and 30 mm/s in head-restrained (black), and freely swimming (grey) larvae (speed 0 mm/s: 84 restrained bouts, 2,427 free-swimming bouts, speed 5 mm/s: 2,748 restrained and 5,092 free-swimming bouts, speed 10 mm/s: 2,698 restrained and 3,334 free-swimming bouts, speed 30 mm/s: 1,472 restrained and 1,631 free-swimming bouts). The inserts show the cumulative distribution function for both the histograms for ease of comparison. Only the last set of histograms (elicited with a 30 mm/s grating) were significantly different from each other (Kolmogorov-Smirnov test, $p<0.01$).

Figure 4. Laser ablation of the nMLF reduces OMR-induced swimming speed
(A) Inset: Head of a larval zebrafish. Image of reticulospinal labeling is overlaid in approximate location. Schematic of reticulospinal neurons in the mid and hindbrain labeled by spinal backfill with large nMLF neurons (red), and control ablation neurons (blue) in some larvae a subset of RoM neurons from the second and third rhombomeres, or in some larvae the Mauthner cells. Scale bar 50 μm. (B) Maximum intensity z-projection of image stacks taken of the nMLF before and four hours after laser ablation. Targeted cells are indicated by red dot. Scale bar 25 μm. (C) Histogram of the probabilities of various kinematic parameters of swimming occurring before (grey; 17 larvae; 1506 bouts), and after (red; same larvae; 806 bouts) ablation of the nMLF. From left to right: the bout duration (ms), the maximum tail-beat frequency (Hz), the bout distance (mm), and the bout speed (mm/s). The cumulative distribution functions pre and post-ablation are plotted in the upper right. The distributions of the two histograms are significantly different in all cases (Kolmogorov-Smirnov test, $p<0.05$ (single asterisk) or $p<0.01$ (double asterisk)). (D) Histogram of swimming speed before (grey; 10 larvae; 1364 bouts), and after (blue; same larvae; 1012 bouts) ablation of control neurons for the same kinematic parameters. The cumulative distribution functions pre and post-ablation are plotted in the upper right, and are not significantly different in any case.

Figure 5. Electrical stimulation of the nMLF elicits swim-like behavior and neural responses modulated by the stimulation intensity
(A) Behavioral responses during midbrain electrical stimulation. (A, left) Image of a larva responding to midbrain electrical stimulation. Electrode position can be seen as well as border of agarose removed to free the tail. Image acquired at 250 Hz, exposure 0.32 ms, maximum intensity z-projection with every two out of three frames removed for clarity. (A, right) Recorded locomotor responses elicited by nMLF stimulation. (B) Calcium activity in the nMLF during electrical stimulation. (B, left). Reference image of nMLF neurons, labeled with Texas Red Dextran, viewed with both bright-field and epifluorescence illumination. Stimulation pipette is outlined and the left MeLc neuron (calcium response shown in panel E) circled. (B, right) Raw

calcium trace from nMLF left MeLc cell during midbrain electrical stimulation, and accompanying stimulus of five trains. (C) Average bout durations from swim-like behavioral responses to midbrain electrical stimulation (0.45 μA) over five different stimulation frequencies (2, 4, 6, 8, 10 pulses per second). n= 13 larvae and 4,373 bouts. Error bars denote the mean +/- SEM. A three-way ANOVA was used to determine statistical significance: frequency of stimulation was significant ($p<0.0001$). In all cases examining behavior, individual larvae were also significantly different from each other ($p<0.0001$). (D) The average maximum tail-beat frequencies calculated per bout and averaged across larvae during bouts elicited by electrical stimulation (n= 13 larvae and 4,373 bouts). Frequency of stimulation significantly modulated maximum TBF ($p<0.0003$). Stimulation parameters and statistical methods identical to those in C. (E) Calcium responses from identifiable nMLF cells to midbrain electrical stimulation for three different currents over five different stimulation frequencies. Maximum $\Delta f/f$ response for the average of all cells across all larvae (n=16 larvae, 101 cells). Error bars denote the mean +/- SEM.

Figure 6. Monitoring activity of the nMLF population with two-photon calcium imaging
(A) Head of a larval zebrafish. The nMLF is located in the magenta rectangle ~140-200 µm from the dorsal surface. Image of reticulospinal labeling including nMLF neurons is overlaid in approximate location. (B) Z-projection of a stack of nMLF neurons. Cells are labeled via spinal injections of calcium green dextran. Cells colored-coded as small (orange), large MeL cells (blue) or large MeM cells (green). (C) Calcium signals recorded in several cells simultaneously. Periods of stimulus presentation are indicated by magenta shaded areas for forward grating motion, and grey shaded areas for backward grating motion. The grating speed in mm/s is indicated above. (D and E) The maximum $\Delta f/f$ calcium response and the latency to the peak of the calcium signal respectively during stimulus presentation as a function of grating speed for the large cells and small cells. Responses were recorded from individual cells and when no significant differences were observed between groups, responses were pooled for clarity. Error bars represent the SEM. Large cells: MeLr (n = 25), MeLc (n = 23), MeLm (n = 6), and MeM (n = 10), All (n = 64). Small cells: left lateral (n = 59), left medial (n = 43), right lateral (n = 57) and right medial (n = 31), All (n = 190). N = 21 larvae. (F) The fraction of active cells during forward moving gratings across grating speeds. Cells were classified as active if their $\Delta f/f$ was above a 10% threshold.

Figure 7. Calcium imaging of nMLF activity in behaving larvae
(A) Image of a larval zebrafish in the two-photon imaging setup while motionless (left) and a projection while performing a slow swim (right). The larval behavior is imaged from below so the round outline visible in the background is the objective above. (B) Sample of data acquired during an experiment. The data shown corresponds to imaging one plane through the nMLF for two minutes, 80 such planes per imaging session per larva with 1 μm separation. In each plane, six 10 s periods of a static grating were interleaved with six 10 s periods of a forward moving grating at 5, 10, or 30 mm/s (shown at top). Each grating speed was repeated twice per plane. In each plane several nMLF cells were visible and their fluorescence traces could be determined (shown in blue). The setup allows simultaneous monitoring of tail movement during calcium imaging (cumulative tail angle is shown in black, see panel D for better resolution). (C) Percentage of bouts elicited by the different grating speeds presented. (D) Tail motion trace for a representative swim bout recorded in the setup. (E) Sensory-triggered calcium responses (top and middle) for each of the four large nMLF cell types have been grouped into repetitions during which larvae performed swim bouts (top) and those during which larvae did not (middle) and color coded for the speed of the grating that was presented (black, blue and red for 5, 10 and 30 mm/s respectively). Motor-triggered responses for the four large cell types are shown in the

bottom, color-coded for the grating speed at which they were elicited. The data shown are the average of all the cells labeled from 20 larvae. (F) Scatter plot for all swim bouts recorded in a sample larva of bout duration versus the maximum calcium response for each of the four large nMLF cell types (MeLr, MeLc, MeLm and MeM in red, blue, green, and black respectively) together with the best fit arising from linear regression. (G) Scatter plot for all swim bouts recorded in a sample larva of maximum tail-beat frequency versus the maximum calcium response for each of the four large nMLF cell types together with the best fit arising from linear regression. (H) Percentage of cells for the four large nMLF cell types that were found to have a significant correlation with bout duration (31/38, 10/18, 2/4, 12/38 from 20 larvae). (I) Percentage of cells for the four large nMLF cell types that were found to have a significant correlation with the maximum TBF (21/38, 16/18, 2/4, 10/38 from 20 larvae).

Figure 8. Schematic model for the nMLF as a center for sensorimotor processing and locomotor drive

This model shows the nMLF as a center for sensorimotor processing and locomotor drive. Olfactory inputs are processed in the forebrain and have been functionally and anatomically linked to a pathway leading to the posterior tuberculum, the MLR, and to reticulospinal cells in closely related model systems. The MLR, if located in the larval zebrafish, would likely send bilateral cholinergic projections to the nMLF. Visual inputs from the retina are relayed to visual processing areas such as the pretectum, from where projections may be relayed to the nMLF (shown in green). There are significant TH and 5-HT projections surrounding the nMLF which could provide a source of neuromodulation. Vestibular inputs may be relayed via the tangential nucleus located next to the ear with projections to the nMLF. Together all of these inputs could be synthesized in the nMLF to direct locomotion. The spinal cord is activated by descending glutamatergic inputs from the reticulospinal cells causing central pattern generators to oscillate, driving locomotor output and receiving proprioceptive feedback. Within the spinal cord (lateral view) there is a dorsal-ventral arrangement of activation with ventral spinal interneurons and motor neurons activated at slow swimming frequencies, and more dorsal recruitment as locomotor intensity must increase. Neurons from the nMLF innervate along a dorsal-ventral gradient in the spinal cord (Wang and McLean, co-submission) which could specify the tonic excitation provided to where it is required in spinal cord to produce a variety of speeds of locomotion. Abbreviations: 5-HT: serotonin, MLR: mesencephalic locomotor region, OB: olfactory bulb, PreT: pretectum, PT: posterior tuberculum, TH: tyrosine hydroxylase. Schematic of reticulospinal cells from (Orger et al., 2008).

References

Ahrens, M.B., Li, J.M., Orger, M.B., Robson, D.N., Schier, A.F., Engert, F., and Portugues, R. (2012). Brain-wide neuronal dynamics during motor adaptation in zebrafish. Nature 485, 471-477.

Ampatzis, K., Song, J., Ausborn, J., and El Manira, A. (2013). Pattern of innervation and recruitment of different classes of motoneurons in adult zebrafish. The Journal of neuroscience : the official journal of the Society for Neuroscience 33, 10875-10886.

Arenzana, F.J., Clemente, D., Sanchez-Gonzalez, R., Porteros, A., Aijon, J., and Arevalo, R. (2005). Development of the cholinergic system in the brain and retina of the zebrafish. Brain research bulletin 66, 421-425.

Arrenberg, A.B., Del Bene, F., and Baier, H. (2009). Optical control of zebrafish behavior with halorhodopsin. Proceedings of the National Academy of Sciences of the United States of America 106, 17968-17973.

Berkowitz, A., Roberts, A., and Soffe, S.R. (2010). Roles for multifunctional and specialized spinal interneurons during motor pattern generation in tadpoles, zebrafish larvae, and turtles. Frontiers in behavioral neuroscience 4, 36.
Bhatt, D.H., McLean, D.L., Hale, M.E., and Fetcho, J.R. (2007). Grading movement strength by changes in firing intensity versus recruitment of spinal interneurons. Neuron 53, 91-102.
Bianco, I.H., Kampff, A.R., and Engert, F. (2011). Prey capture behavior evoked by simple visual stimuli in larval zebrafish. Frontiers in systems neuroscience 5, 101.
Bianco, I.H., Ma, L.H., Schoppik, D., Robson, D.N., Orger, M.B., Beck, J.C., Li, J.M., Schier, A.F., Engert, F., and Baker, R. (2012). The tangential nucleus controls a gravito-inertial vestibulo-ocular reflex. Current biology : CB 22, 1285-1295.
Bilotta, J. (2000). Effects of abnormal lighting on the development of zebrafish visual behavior. Behavioural Brain Research 116, 81-87.
Borla, M.A., Palecek, B., Budick, S., rsquo, and Malley, D.M. (2002). Prey Capture by Larval Zebrafish: Evidence for Fine Axial Motor Control. Brain, Behavior and Evolution 60, 207-229.
Brocard, F., Ryczko, D., Fenelon, K., Hatem, R., Gonzales, D., Auclair, F., and Dubuc, R. (2010). The transformation of a unilateral locomotor command into a symmetrical bilateral activation in the brainstem. The Journal of neuroscience : the official journal of the Society for Neuroscience 30, 523-533.
Brustein, E., Chong, M., Holmqvist, B., and Drapeau, P. (2003). Serotonin patterns locomotor network activity in the developing zebrafish by modulating quiescent periods. Journal of neurobiology 57, 303-322.
Buchanan, J.T., and Grillner, S. (1987). Newly identified 'glutamate interneurons' and their role in locomotion in the lamprey spinal cord. Science 326, 312-314.
Budick, S.A., and O'Malley, D.M. (2000). Locomotor repertoire of the larval zebrafish: swimming, turning and prey capture. The Journal of experimental biology 203, 2565–2579.
Burgess, H.A., and Granato, M. (2007). Modulation of locomotor activity in larval zebrafish during light adaptation. The Journal of experimental biology 210, 2526-2539.
Burrill, J.D., and Easter, S.S. (1994). Development of the Retinofugal Projections in the Embryonic and Larval Zebrafish (Brachydanio rerio). J Comp Neurol 346, 583-600.
Cabelguen JM, B.-L.C., Dubuc R (2003). Bimodal Locomotion Elicited by Electrical Stimulation of the Midbrain in the Salamander Notophthalmus viridescens. The Journal of neuroscience : the official journal of the Society for Neuroscience 23, 2434 –2439.
Crone, S.A., Zhong, G., Harris-Warrick, R., and Sharma, K. (2009). In mice lacking V2a interneurons, gait depends on speed of locomotion. The Journal of neuroscience : the official journal of the Society for Neuroscience 29, 7098-7109.
Dale, N. (2002). Resetting Intrinsic Purinergic Modulation of Neural Activity: An Associative Mechanism? The Journal of neuroscience : the official journal of the Society for Neuroscience 22, 10461-10469.
Deliagina, T.G., Zelenin, P.V., and Orlovsky, G.N. (2002). E ncoding and decoding of reticulospinal commands. Brain research reviews 40, 166-177.
Derjean D, M.A., Atallah E, St-Pierre M, Auclair F, Chang S, Ren X, Zielinski B, Dubuc R (2010). A Novel Neural Substrate for the Transformation of Olfactory Inputs into Motor Output. PLoS Biology 8, 1-11.
Gahtan, E., and O'Malley, D.M. (2003). Visually guided injection of identified reticulospinal neurons in zebrafish: a survey of spinal arborization patterns. J Comp Neurol 459, 186-200.

Gahtan, E., Tanger, P., and Baier, H. (2005). Visual prey capture in larval zebrafish is controlled by identified reticulospinal neurons downstream of the tectum. The Journal of neuroscience : the official journal of the Society for Neuroscience 25, 9294-9303.
Gosgnach, S., Lanuza, G.M., Butt, S.J., Saueressig, H., Zhang, Y., Velasquez, T., Riethmacher, D., Callaway, E.M., Kiehn, O., and Goulding, M. (2006). V1 spinal neurons regulate the speed of vertebrate locomotor outputs. Nature 440, 215-219.
Goulding, M. (2009). Circuits controlling vertebrate locomotion: moving in a new direction. Nature reviews Neuroscience 10, 507-518.
Green, M.H., Ho, R.K., and Hale, M.E. (2011). Movement and function of the pectoral fins of the larval zebrafish (Danio rerio) during slow swimming. The Journal of experimental biology 214, 3111-3123.
Grillner, S., Robertson, B., and Stephenson-Jones, M. (2013). The evolutionary origin of the vertebrate basal ganglia and its role in action selection. J Physiol 591, 5425-5431.
Haehnel, M., Taguchi, M., and Liao, J.C. (2012). Heterogeneity and dynamics of lateral line afferent innervation during development in zebrafish (Danio rerio). J Comp Neurol 520, 1376-1386.
Hagglund, M., Borgius, L., Dougherty, K.J., and Kiehn, O. (2010). Activation of groups of excitatory neurons in the mammalian spinal cord or hindbrain evokes locomotion. Nature neuroscience 13, 246-252.
Hale, M.E., Ritter, D.A., and Fetcho, J.R. (2001). A Confocal Study of Spinal Interneurons in Living Larval Zebrafish. J Comp Neurol 437, 1-16.
Huang, K.H., Ahrens, M.B., Dunn, T.W., and Engert, F. (2013). Spinal projection neurons control turning behaviors in zebrafish. Current biology : CB 23, 1566-1573.
Jordan, L.M. (1998). Initiation of locomotion in mammals. Annals of the New York Academy of Sciences 860, 83-93.
Kashin SM, F.A., Orlovsky GN (1974). Locomotion of the fish evoked by electrical stimulation of the brain. Brain Res 82, 41-47.
Kay, J.N., Finger-Baier, K.C., Roeser, T., Staub, W., Baier, H. (2001). Retinal Ganglion Cell Genesis Requires lakritz, a Zebrafish atonal Homolog. Neuron 30, 725-736.
Kimmel, C.B., Powell, S.L., and Metcalfe, W.K. (1982). Brain Neurons Which Project to the Spinal Cord in Young Larvae of the Zebrafish. J Comp Neurol 205, 112-127.
Kimura, Y., Satou, C., Fujioka, S., Shoji, W., Umeda, K., Ishizuka, T., Yawo, H., and Higashijima, S.I. (2013). Hindbrain V2a Neurons in the Excitation of Spinal Locomotor Circuits during Zebrafish Swimming. Current biology : CB.
Kohashi, T., and Oda, Y. (2008). Initiation of Mauthner- or non-Mauthner-mediated fast escape evoked by different modes of sensory input. The Journal of neuroscience : the official journal of the Society for Neuroscience 28, 10641-10653.
Koyama, M., Kinkhabwala, A., Satou, C., Higashijima, S., and Fetcho, J.R. (2011). Mapping a sensory-motor network onto a structural and functional ground plan in the hindbrain. PNAS 108, 1170-1175.
Kubo, F., Hablitzel, B., Dal Maschio, M., Driever, W., Baier, H., and Arrenberg, A.B. (2014). Functional Architecture of an Optic Flow-Responsive Area that Drives Horizontal Eye Movements in Zebrafish. Neuron 81, 1344-1359.
Li, W.C., Perrins, R., Walford, A., and Roberts, A. (2003). The neuronal targets for GABAergic reticulospinal inhibition that stops swimming in hatchling frog tadpoles. Journal of comparative physiology A, Neuroethology, sensory, neural, and behavioral physiology 189, 29-37.

Maaswinkel, H., and Li, L. (2003). Spatio-temporal frequency characteristics of the optomotor response in zebrafish. Vision Research 43, 21-30.
Masai, I.L., Z. Yamaguchi, M. Komori, A. Nakata, A. Nishiwaki, Y. Wada, H. Tanaka, H. Nojima, Y. Hammerschmidt, M. Wilson, S.W. Okamoto, H. (2003). N-cadherin mediates retinal lamination, maintenance of forebrain compartments and patterning of retinal neurites. Development 130, 2479-2494.
McDearmid, J.R., and Drapeau, P. (2006). Rhythmic motor activity evoked by NMDA in the spinal zebrafish larva. Journal of neurophysiology 95, 401-417.
McLean, D.L., Fan, J., Higashijima, S., Hale, M.E., and Fetcho, J.R. (2007). A topographic map of recruitment in spinal cord. Nature 446, 71-75.
McLean, D.L., and Fetcho, J.R. (2004). Relationship of tyrosine hydroxylase and serotonin immunoreactivity to sensorimotor circuitry in larval zebrafish. J Comp Neurol 480, 57-71.
McLean, D.L., Masino, M.A., Koh, I.Y., Lindquist, W.B., and Fetcho, J.R. (2008). Continuous shifts in the active set of spinal interneurons during changes in locomotor speed. Nature neuroscience 11, 1419-1429.
Menelaou, E., and McLean, D.L. (2012). A gradient in endogenous rhythmicity and oscillatory drive matches recruitment order in an axial motor pool. The Journal of neuroscience : the official journal of the Society for Neuroscience 32, 10925-10939.
Muto, A., Orger, M.B., Wehman, A.M., Smear, M.C., Kay, J.N., Page-McCaw, P.S., Gahtan, E., Xiao, T., Nevin, L.M., Gosse, N.J., et al. (2005). Forward genetic analysis of visual behavior in zebrafish. PLoS genetics 1, e66.
Neuhauss, S.C.F., Biehlmaier, O., Seeliger, M.W., Das, T., Kohler, K., Harris, W.A., and Baier, H. (1999). Genetic Disorders of Vision Revealed by a Behavioral Screen of 400 Essential Loci in Zebrafish. J Neurosci 19, 8603-8615.
O'Malley, D.M., Kao, Y.H., and Fetcho, J.R. (1996). Imaging the Functional Organization of Zebrafish Hindbrain Segments during Escape Behaviors. Neuron 17, 1145–1155.
Orger, M.B., Kampff, A.R., Severi, K.E., Bollmann, J.H., and Engert, F. (2008). Control of visually guided behavior by distinct populations of spinal projection neurons. Nature neuroscience 11, 327-333.
Orger, M.B., Smear, M.C., Anstis, S.M., and Baier, H. (2000). Perception of Fourier and non-Fourier motion by larval zebrafish. Nature neuroscience 3, 1128-1133.
Portugues, R., and Engert, F. (2009). The neural basis of visual behaviors in the larval zebrafish. Current opinion in neurobiology 19, 644-647.
Portugues, R., and Engert, F. (2011). Adaptive locomotor behavior in larval zebrafish. Frontiers in systems neuroscience 5, 72.
Portugues, R., Feierstein, C.E., Engert, F., and Orger, M.B. (2014). Whole-brain activity maps reveal stereotyped, distributed networks for visuomotor behavior. Neuron 81, 1328-1343.
Ritter, D.A., Bhatt, D.H., and Fetcho, J.R. (2001). In Vivo Imaging of Zebrafish Reveals Differences in the Spinal Networks for Escape and Swimming Movements. The Journal of neuroscience : the official journal of the Society for Neuroscience 21, 8956–8965.
Roberts, A., Li, W.C., and Soffe, S.R. (2010). How neurons generate behavior in a hatchling amphibian tadpole: an outline. Frontiers in behavioral neuroscience 4, 16.
Roberts, A., Li, W.C., Soffe, S.R., and Wolf, E. (2008). Origin of excitatory drive to a spinal locomotor network. Brain research reviews 57, 22-28.
Robles, E., Smith, S.J., and Baier, H. (2011). Characterization of genetically targeted neuron types in the zebrafish optic tectum. Frontiers in neural circuits 5, 1.

Roeser, T., and Baier, H. (2003). Visuomotor Behaviors in Larval Zebrafish after GFP-Guided Laser Ablation of the Optic Tectum. The Journal of neuroscience : the official journal of the Society for Neuroscience 23, 3726-3734.
Sankrithi, N.S., and O'Malley, D.M. (2010). Activation of a multisensory, multifunctional nucleus in the zebrafish midbrain during diverse locomotor behaviors. Neuroscience 166, 970-993.
Sato, T., Hamaoka, T., Aizawa, H., Hosoya, T., and Okamoto, H. (2007). Genetic single-cell mosaic analysis implicates ephrinB2 reverse signaling in projections from the posterior tectum to the hindbrain in zebrafish. The Journal of neuroscience : the official journal of the Society for Neuroscience 27, 5271-5279.
Shik ML, O.G., Severin FV (1966). Control of walking by means of electrical stimulation of the mid-brain. Biophysics 11, 756-765.
Steeves, J., Sholomenko, GN., Webster, DMS. (1986). Stimulation of the pontomedullary reticular formation initiates locomotion in decerebrate birds. Brain Res 401, 205-212.
Talpalar, A.E., and Kiehn, O. (2010). Glutamatergic mechanisms for speed control and network operation in the rodent locomotor CpG. Frontiers in neural circuits 4.
Tay, T.L., Ronneberger, O., Ryu, S., Nitschke, R., and Driever, W. (2011). Comprehensive catecholaminergic projectome analysis reveals single-neuron integration of zebrafish ascending and descending dopaminergic systems. Nature communications 2, 171.
Westphal, R.E., and O'Malley, D.M. (2013). Fusion of locomotor maneuvers, and improving sensory capabilities, give rise to the flexible homing strikes of juvenile zebrafish. Frontiers in neural circuits 7, 108.
Wiggin, T.D., Anderson, T.A., Eian, J., Peck, J.H., Masino, M.A. (2012). Episodic swimming in the larval zebrafish is generated by a spatially distributed spinal network with modular functional organization. Journal of neurophysiology 108, 925-934.
Wyart, C., Del Bene, F., Warp, E., Scott, E.K., Trauner, D., Baier, H., and Isacoff, E.Y. (2009). Optogenetic dissection of a behavioural module in the vertebrate spinal cord. Nature 461, 407-410.

FIGURE 1

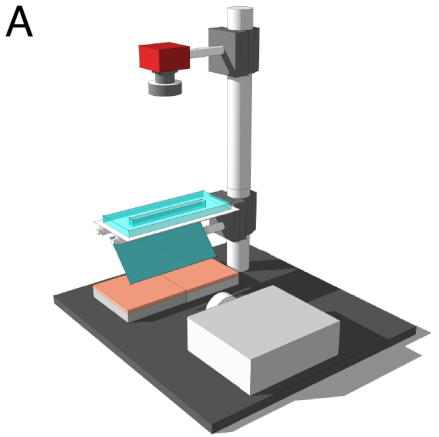
A

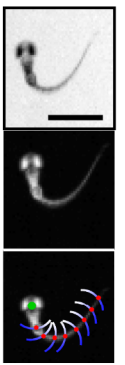
B

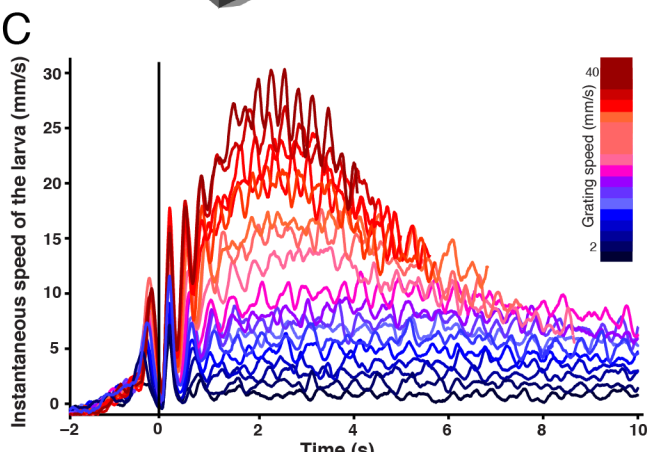
C
Instantaneous speed of the larva (mm/s)
Time (s)
Grating speed (mm/s)
40
2

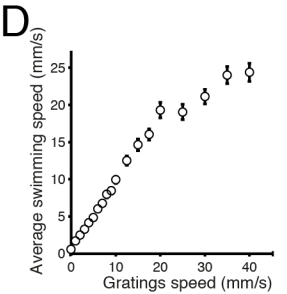
D
Average swimming speed (mm/s)
Gratings speed (mm/s)

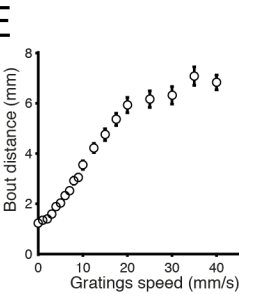
E
Bout distance (mm)
Gratings speed (mm/s)

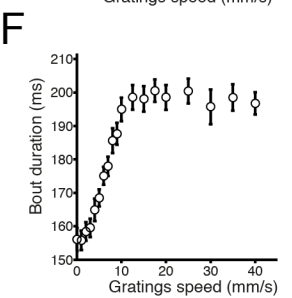
F
Bout duration (ms)
Gratings speed (mm/s)

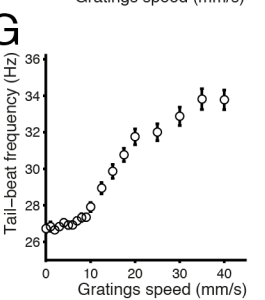
G
Tail–beat frequency (Hz)
Gratings speed (mm/s)

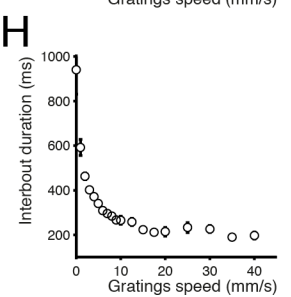
H
Interbout duration (ms)
Gratings speed (mm/s)

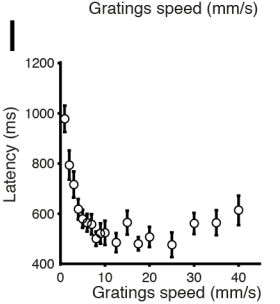
I
Latency (ms)
Gratings speed (mm/s)

FIGURE 2

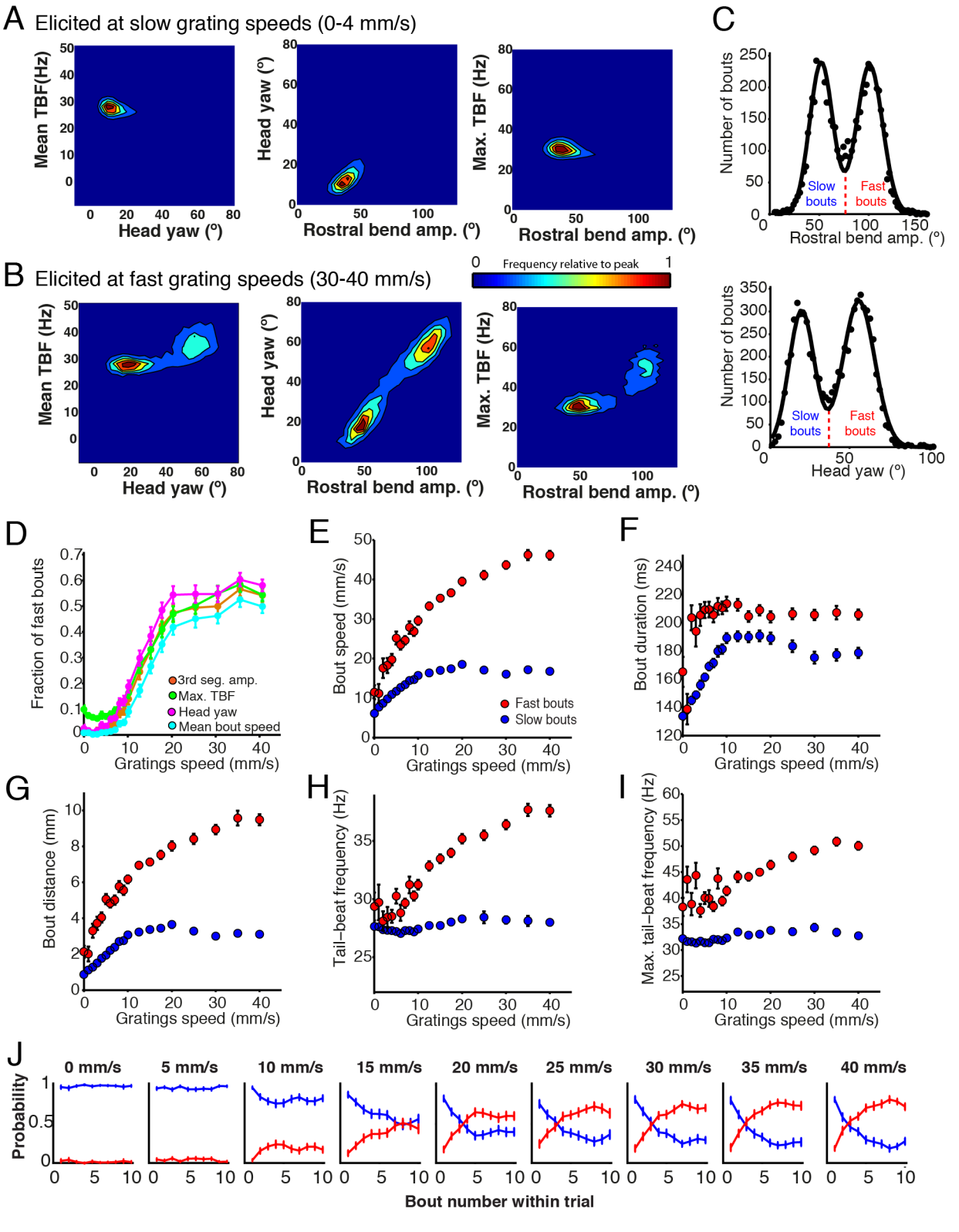
A
Elicited at slow grating speeds (0-4 mm/s)
Mean TBF(Hz)
Head yaw (°)
Head yaw (°)
Rostral bend amp. (°)
Max. TBF (Hz)
Rostral bend amp. (°)
B
Elicited at fast grating speeds (30-40 mm/s)
0
Frequency relative to peak
1
Mean TBF (Hz)
Head yaw (°)
Head yaw (°)
Rostral bend amp. (°)
Max. TBF (Hz)
Rostral bend amp. (°)
C
Number of bouts
Slow bouts
Fast bouts
Rostral bend amp. (°)
Number of bouts
Slow bouts
Fast bouts
Head yaw (°)
D
Fraction of fast bouts
3rd seg. amp.
Max. TBF
Head yaw
Mean bout speed
Gratings speed (mm/s)
E
Bout speed (mm/s)
Fast bouts
Slow bouts
Gratings speed (mm/s)
F
Bout duration (ms)
Gratings speed (mm/s)
G
Bout distance (mm)
Gratings speed (mm/s)
H
Tail–beat frequency (Hz)
Gratings speed (mm/s)
I
Max. tail–beat frequency (Hz)
Gratings speed (mm/s)
J
0 mm/s
5 mm/s
10 mm/s
15 mm/s
20 mm/s
25 mm/s
30 mm/s
35 mm/s
40 mm/s
Probability
Bout number within trial

FIGURE 3

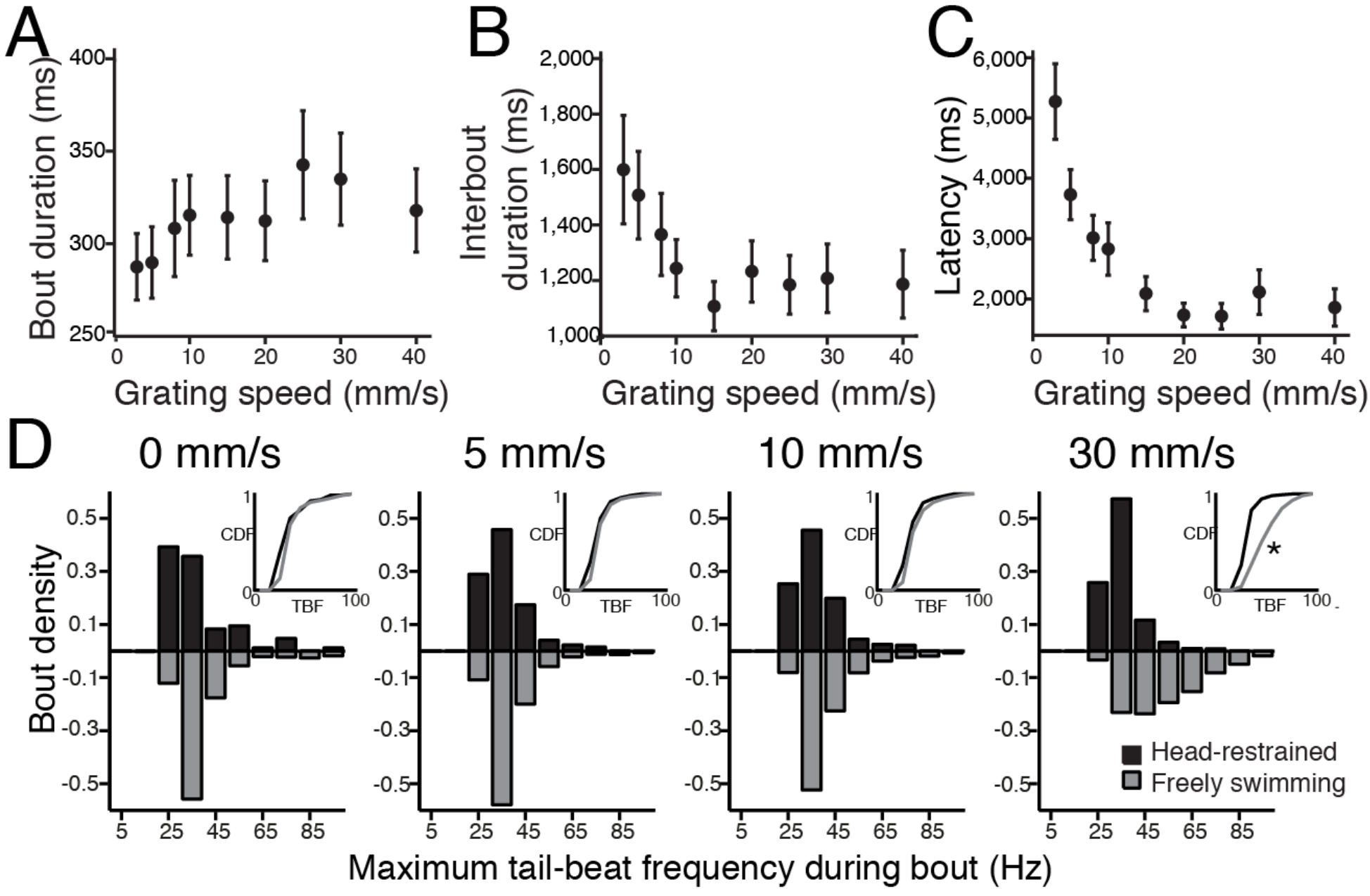
A
Bout duration (ms)
400
350
300
250
0
10
20
30
40
Grating speed (mm/s)
B
Interbout duration (ms)
2,000
1,800
1,600
1,400
1,200
1,000
0
10
20
30
40
Grating speed (mm/s)
C
Latency (ms)
6,000
5,000
4,000
3,000
2,000
0
10
20
30
40
Grating speed (mm/s)
D
0 mm/s
5 mm/s
10 mm/s
30 mm/s
Bout density
0.5
0.3
0.1
-0.1
-0.3
-0.5
CDF
1
0
0
TBF
100
*
5
25
45
65
85
Head-restrained
Freely swimming
Maximum tail-beat frequency during bout (Hz)

FIGURE 4

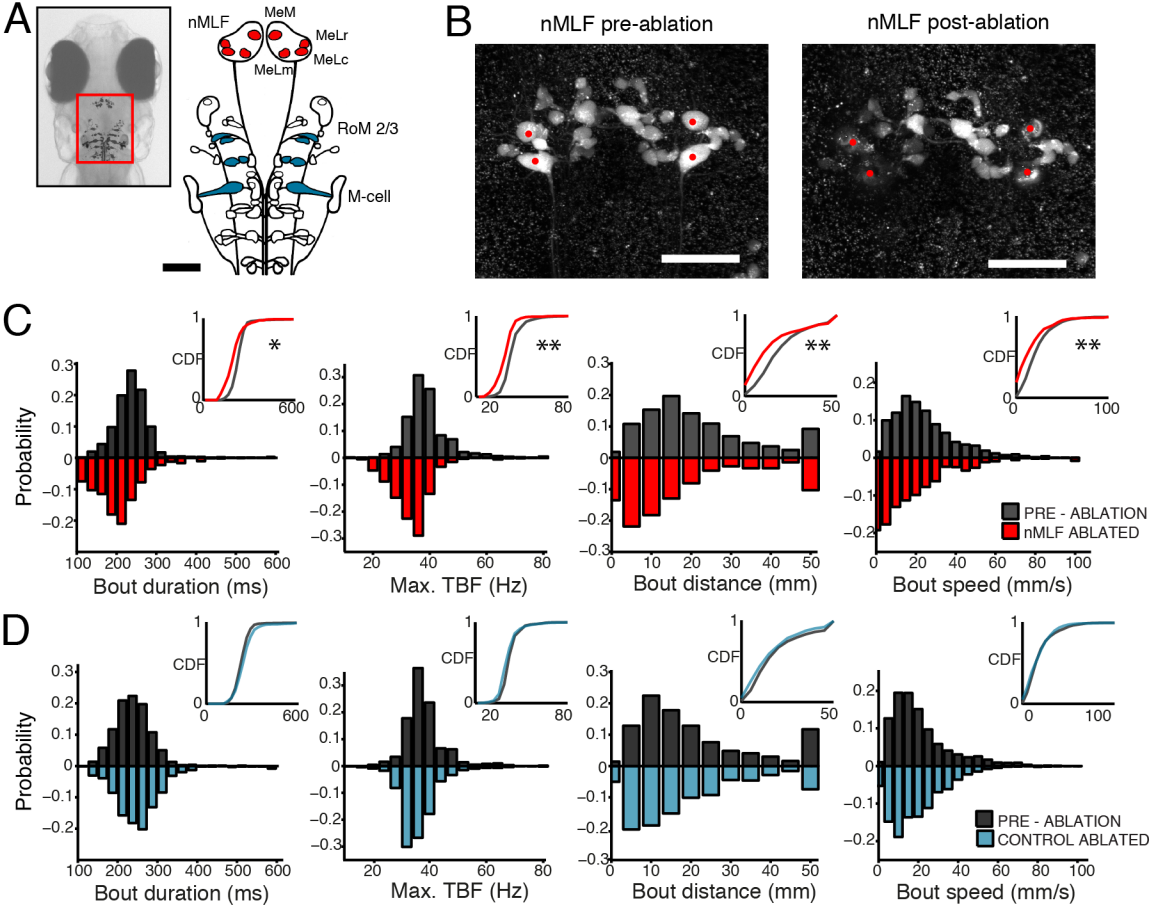
A
nMLF
MeM
MeLr
MeLc
MeLm
RoM 2/3
M-cell
B
nMLF pre-ablation
nMLF post-ablation
C
Probability
CDF
*
**
**
**
Bout duration (ms)
Max. TBF (Hz)
Bout distance (mm)
Bout speed (mm/s)
PRE - ABLATION
nMLF ABLATED
D
Probability
CDF
Bout duration (ms)
Max. TBF (Hz)
Bout distance (mm)
Bout speed (mm/s)
PRE - ABLATION
CONTROL ABLATED

FIGURE 5

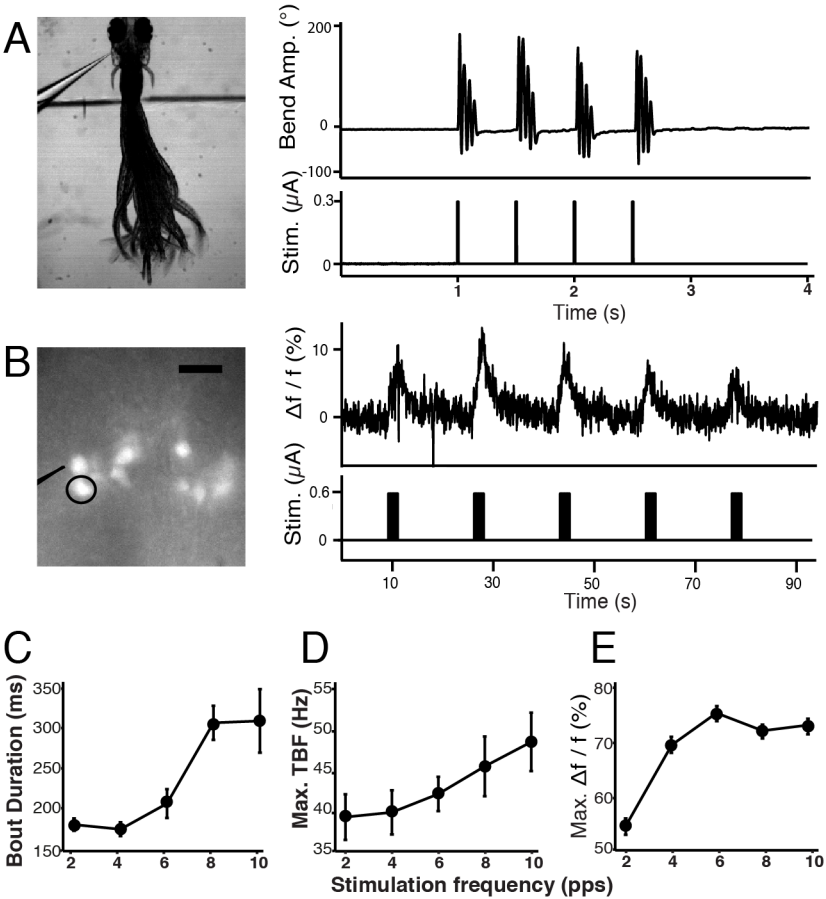
A
Bend Amp. (°)
200
0
-100
Stim. (μA)
0.3
0
1
2
3
4
Time (s)
B
Δf / f (%)
10
0
Stim. (μA)
0.6
0
10
30
50
70
90
Time (s)
C
Bout Duration (ms)
350
300
250
200
150
2
4
6
8
10
D
Max. TBF (Hz)
55
50
45
40
35
2
4
6
8
10
E
Max. Δf / f (%)
80
70
60
50
2
4
6
8
10
Stimulation frequency (pps)

FIGURE 6

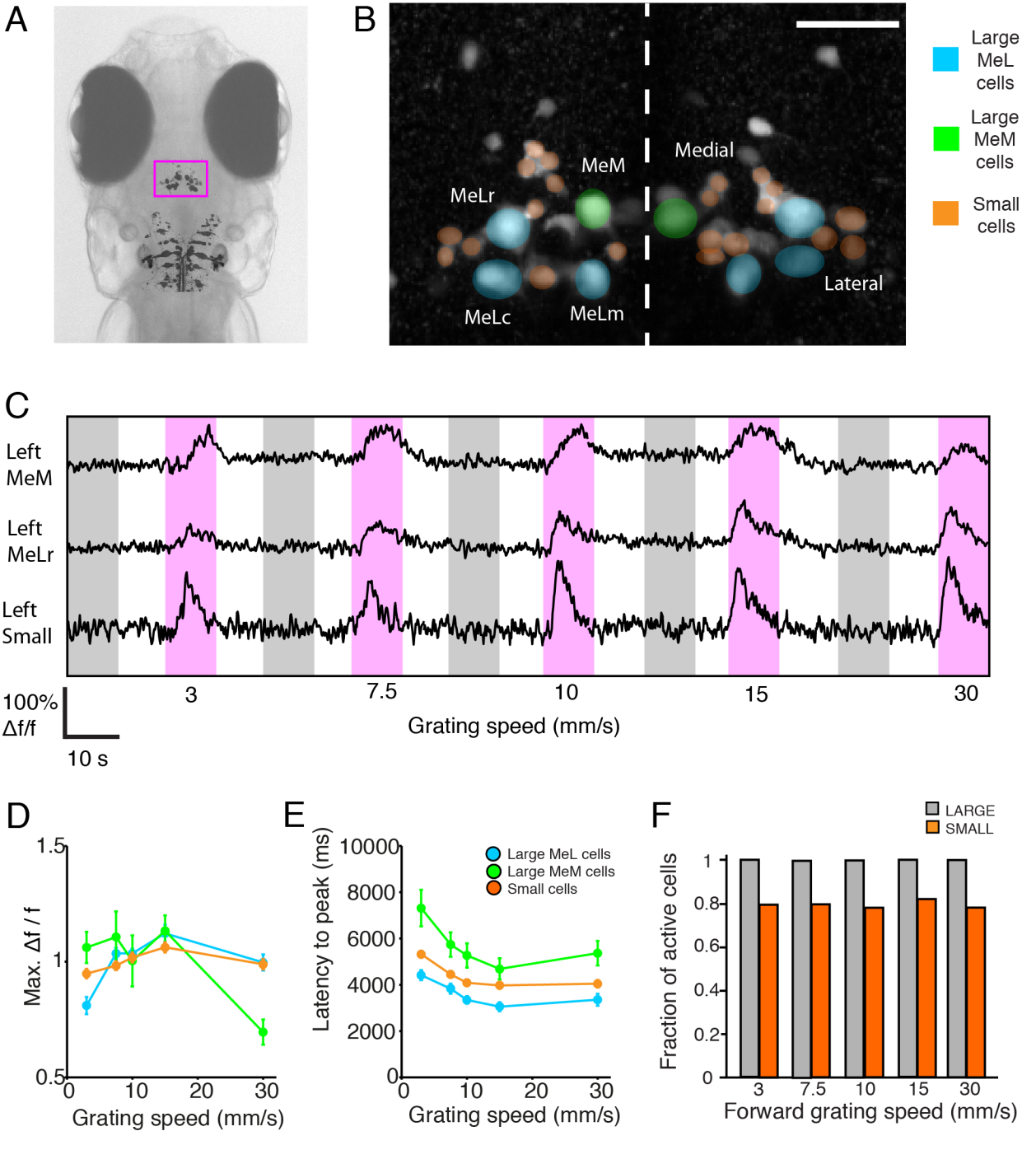
A
B
MeM
MeLr
MeLc
MeLm
Medial
Lateral
Large MeL cells
Large MeM cells
Small cells
C
Left MeM
Left MeLr
Left Small
100% Δf/f
10 s
3
7.5
10
15
30
Grating speed (mm/s)
D
Max. Δf / f
Grating speed (mm/s)
E
Latency to peak (ms)
Large MeL cells
Large MeM cells
Small cells
Grating speed (mm/s)
F
LARGE
SMALL
Fraction of active cells
Forward grating speed (mm/s)

FIGURE 7

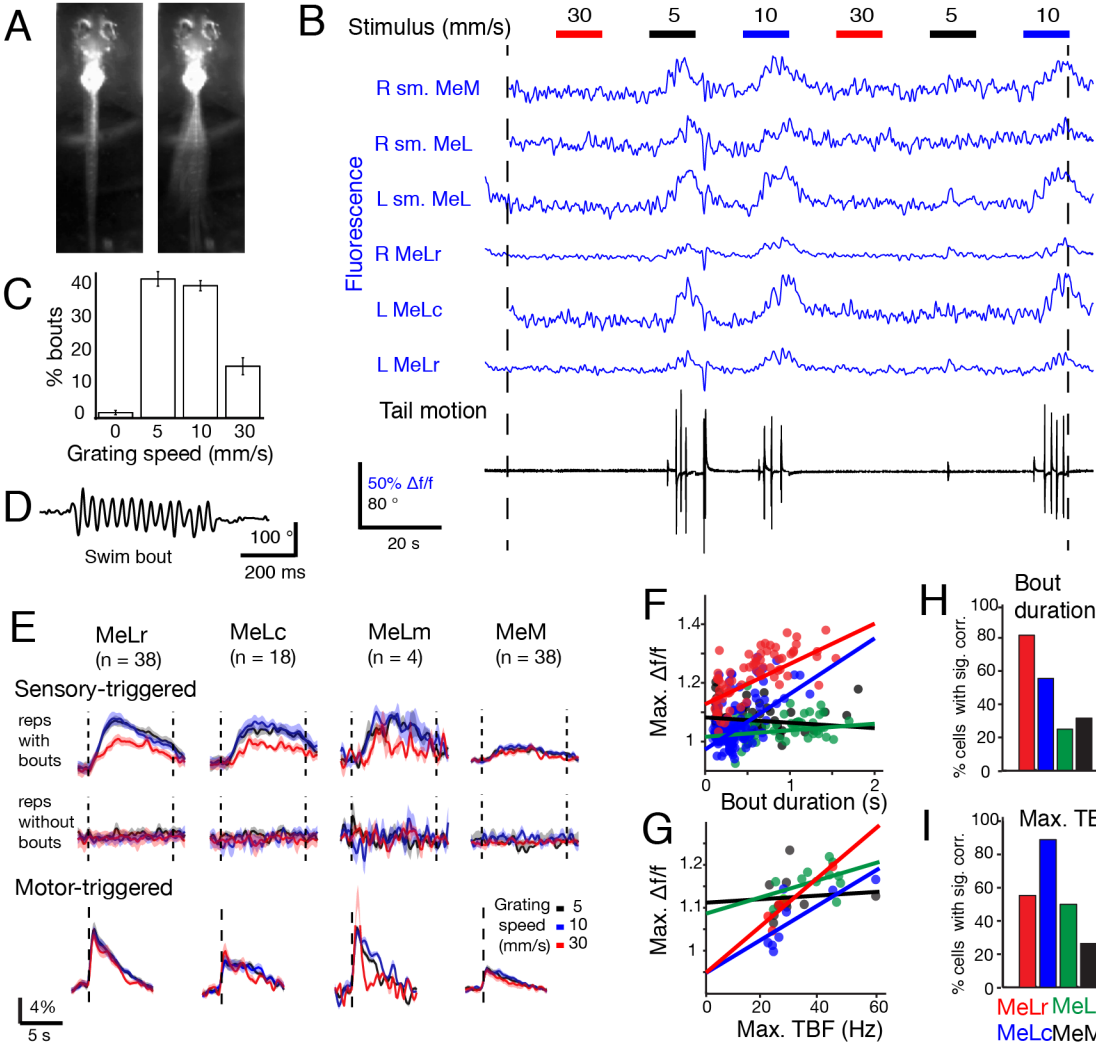
A
B
Stimulus (mm/s)
30
5
10
30
5
10
R sm. MeM
R sm. MeL
L sm. MeL
R MeLr
L MeLc
L MeLr
Fluorescence
Tail motion
50% Δf/f
80 °
20 s
C
% bouts
40
30
20
10
0
0
5
10
30
Grating speed (mm/s)
D
Swim bout
100 °
200 ms
E
MeLr
(n = 38)
MeLc
(n = 18)
MeLm
(n = 4)
MeM
(n = 38)
Sensory-triggered
reps
with
bouts
reps
without
bouts
Motor-triggered
Grating
speed
(mm/s)
5
10
30
4%
5 s
F
Max. Δf/f
1.4
1.2
1
0
1
2
Bout duration (s)
G
Max. Δf/f
1.2
1.1
1
0
20
40
60
Max. TBF (Hz)
H
Bout
duration
% cells with sig. corr.
100
80
60
40
20
0
I
Max. TBF
% cells with sig. corr.
100
80
60
40
20
0
MeLr
MeLm
MeLc
MeM

FIGURE 8

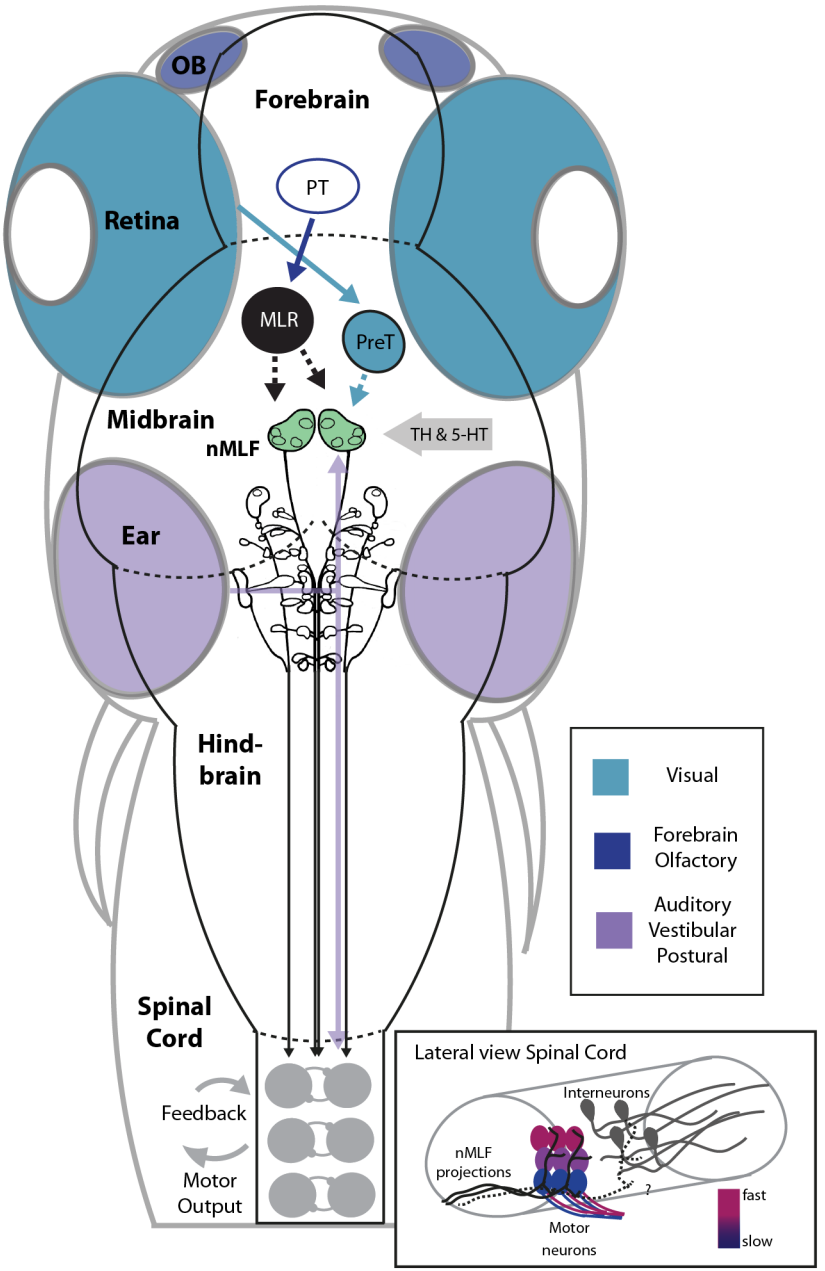
OB
Forebrain
PT
Retina
MLR
PreT
Midbrain
nMLF
TH & 5-HT
Ear
Hind-
brain
Visual
Forebrain
Olfactory
Auditory
Vestibular
Postural
Spinal
Cord
Feedback
Motor
Output
Lateral view Spinal Cord
Interneurons
nMLF
projections
?
Motor
neurons
fast
slow

Supplementary Material
The supplementary material contains 11 figures, three movies, and additional experimental procedures.

Figure S1. Probability of bout type across grating speeds
In these plots of rostral bend amplitude vs, head yaw, we see the probability of a bout falling within that parameter space across all grating speeds tested, from 0 to 40 mm/s. We can see the slow (lower left) cluster shift, and the emergence of the fast (top right) beginning at 12.5 mm/s and increasing in intensity as faster grating speeds are shown.

Figure S2. Method of bout categorization and clustering
We divided all bouts into groups by setting a fixed threshold based on kinematic parameters. We calculated this threshold (dotted line) by fitting a binormal function to the fast trial pool distribution of the rostral bend amplitude and calculating the minimum between the two maximums of the distribution. We observed that bouts with high rostral bend amplitude are correlated with high bout speeds (fast bouts) while bouts with low values of amplitude normally have slow bout speeds (slow bouts). This principle applies to separating forward bouts from turns as well.

Figure S3. Behavioral effects of laser ablation on different neuronal populations plotted against grating speed
Larvae were recorded swimming to different speeds of OMR gratings before and after laser ablation of specific populations: either (A) nMLF neurons, (B) RoM neurons, or (C) both Mauthner cells. Pre-ablation data is plotted in grey for each group and post-ablation data is plotted in color for the average bout parameters: bout speed (mm/s), maximum tail-beat frequency (Hz), bout duration (ms), and bout distance (mm). Larvae with nMLF neurons ablated: n= 17 larvae, 1506 pre bouts, 860 post bouts. Larvae with RoM neurons ablated: n= 7 larvae, 771 pre bouts, 569 post bouts. Larvae with both Mauthner cells ablated: n= 3 larvae, 593 pre bouts, 443 post bouts. Error bars are the standard error of the mean.

Figure S4. Effect of stimulation pipette proximity on locomotor and nMLF calcium responses
(A) Reference image including Texas Red Dextran-labeled nMLF cells and location of the stimulation pipette (red dashed line). Note that the pipette tip is almost touching the bright cell at the left edge of the nMLF (generally outlined by black dashed line). Scale bar is 50 µm. (B) Reference image for a pipette tip at a remote location from the same larva as in A, same scale. (C) Number of bouts elicited in two seconds of stimulation plotted against pipette distance from the edge of the original cell of stimulation. (D) Peak Δf/f in two seconds of stimulation plotted against pipette distance from the edge of the original cell of stimulation**.** n= 10 larvae which contributed to data on all panels.

Figure S5. Electrophysiology reveals nMLF large cell firing increases with grating speed
(A) Bright-field and fluorescent image of the nMLF neurons. Arrow indicates the pipette's location, white dotted line approximates the midline. Rostral is at the top of the image. (B) Example trace of a targeted loose-patch recording from a right MeLr nMLF cell. Each trial recorded voltage over 27 seconds, with grating motion initiated at 9 s and returning to static at 18 s (red dotted lines). This example was recorded during 15mm/s grating speed. (C) Enlargement of two individual spikes from trace shown in B. (D) Raster-gram of a single cell for 60 consecutive trials, red dotted lines indicate initiation and ceasing of grating motion (moving at 15 mm/s for these trials). (E) Average time until the first spike is recorded following initiation of grating motion (n=11 larvae) vs. grating speed for all four speeds tested. Error bars are the

standard error of the mean. (F) Filtered instantaneous firing rate averaged over 11 larvae (approximately 745 trials per speed). Blue trace represents 3 mm/s, green = 7.5 mm/s, orange = 15 mm/s, red = 30 mm/s with red dotted lines indicating initiation and cessation of grating motion.

Figure S6. Correction of motion artifact during calcium imaging
(A) Top: Motion correction applied to individual frames acquired during imaging a single z-plane (864 frames, two minutes, Experimental procedures). Bottom shows zoomed in version between the two dashed red lines in the top graph. Two different metrics for motion correction are shown: in black we see distance moved from previous frame, whereas in red we see distance moved from the average frame in the plane. The vertical dashed blue lines correspond to the frames shown below in B. (B) Eight images showing the frames acquired while imaging the plane shown in A above. The anatomy is the sum of all the frames in the plane and is used as the reference to align all the frames acquired in this plane to. The following seven images show individual frames. The pre-alignment frame (green) is shown superimposed with the post-alignment frame (magenta). (C) The average calcium traces from Figure 7E are shown alongside the average motion correction traces in red.

Figures S7. The calcium activity observed in nMLF cells coincides with locomotor output even in a paralyzed fictive preparation
In this experiment, large identifiable nMLF cells loaded with calcium green dextran were imaged in paralyzed larvae where ventral root activity was recorded as a read out of fictive locomotion. (A) Top: Calcium activity recorded from two nMLF neurons, both MeM cells, morphology shown at right. Middle: Smoothed and filtered firing rate of ventral root output. Bottom: Power (maximum-minimum) calculated from raw ventral root recording. Red asterisk marks the ventral root bout expanded at right. Red asterisk on bout trace represents burst expanded above. In all three panels red-dotted lines mark the time of grating motion. (B) Left: Histogram of recorded spikes from ventral root recordings across all trials (30 ms bins, n = 4 larvae and 28 trials). Right: Average $\Delta F/F$ response from those same trials separated by cell type (left and right identifiable cells were pooled by cell type. MeLr in red (n=35), MeLc in blue (n=38), MeLm in green (n=7), and MeM cells in black (n=12)). Note that during each trial bouts did not always occur at the same points during the trial, however, on average one can observe the most consistent response immediately following the start of grating motion. Each trial was treated independently, rather than averaged by larva, since the number of trials was limited due to the technical difficulty of the experiment.

Figure S8. Proportion of maneuvers exhibited by restrained larvae under the two-photon
Calcium responses in the four large nMLF cell types triggered on four different behaviors: swim bouts, swim bouts which transition into struggles, turns, and struggles (the fraction of all swim bouts accounted for by each individual behavior is shown as a percentage +/- S.E.M.). The behavior y-axis of 100 degrees cumulative tail angle applies to all behavioral traces except the struggle, which is 200 degrees.

Figure S9. Control of significance of R-squared value of the scatter plots in Figure 7
For each scatter plot (x_i, y_i) {i=1,...,n, where n is the total number of swim bouts performed while the cell was being imaged} we computed 1000 controls by randomly permuting the y coordinates: $(x_i, \text{permute}(y_i))$, performing linear regression on each control and then plotted a histogram of the R-squared values of the controls. A correlation was deemed significant if its R-squared value was higher than the 95-th percentile of the R-squared values of its associated 1000 controls. The four histograms shown here correspond to the four cells shown in Figure 7F.

Figure S10. Imaging of retinal ganglion cell projections alongside reticulospinal neurons shows no evidence of direct connections
Transgenic larvae expressing a green fluorescent protein (Dendra) under a driver for retinal ganglion cells (Ath5) via the Gal4/UAS expression system were injected with texas-red dextran to label reticulospinal cells and then imaged at high resolution by two-photon microscopy. (A) Shows a wide view of the head, with the auto-fluorescence in the eyes visible as yellow at the top of the image. Skin auto-fluorescence is also visible, mostly in the green channel. Rostral is at the top, scale bar is 50 µm. (B) A more detailed view, the images move sequentially from dorsal to ventral with the z-position listed in µm on each individual panel. The majority of the retinal ganglion cell projections are dorsal to the position of the nMLF and its dendrites. Rostral is at the top, scale bar is 20 µm. Ath5:Gal4;UAS:Dendra larvae were a generous gift from Dr. Filippo Del Bene, Institut Curie. UAS:Dendra was the same construct used in Arrenberg, Del Bene, and Baier, *PNAS*, 2009.

Figure S11. Minimal damage to surrounding cells during laser ablation
To assess the damage caused to surrounding cells during the laser ablation procedure, we backfilled reticulospinal neurons with texas-red dextran (red) in transgenic larvae expressing GCaMP5G panneuronally (green) (Ahrens, Orger, Robson, Li, and Keller. *Nat. Methods.* 2013). These GCaMP expressing neurons are known to fluoresce for an extended period when damaged. We found very minimal and localized damage sites surrounding successful ablation of single neurons (n= 3 larvae). Scale bar is 20 µm.

Movie S1. Fast bouts vs. slow bouts
Movie showing a sample fast bout (red) and a sample slow bout (blue) as reconstructed from the freely swimming behavioral tracking data.

Movie S2. Large nMLF neurons labeled in a reticulospinal stack
Movie is an image stack of reticulospinal neurons backfilled with dextran with pseudocolored labels overlayed with the large nMLF neurons discussed in this paper. The movie is moving from dorsal to ventral, and the play-rate is 10 Hz.

Movie S3. Head-restrained swimming during *in vivo* two-photon calcium imaging
Movie showing a larva's behavior during 40 seconds of an imaging experiment (4X real-time). The stimulus shown is represented by the moving grating below: four 10 s periods of a grating moving at 0, 10, 0 and 5 mm/s respectively. The image is taken from below such that the circular object in the background corresponds to the objective. The laser can be seen scanning over the head of the larva.

Supplementary Experimental Procedures
Free-swimming behavioral assay
Following background subtraction and inversion, the image was smoothed with a two-dimensional spatial boxcar filter, and the global maximum determined. This point always lies approximately between the larva’s eyes. This point was then used to seed a flood fill on a thresholded version of the image, and the center of mass of the resulting shape which defines a consistent location on the larva's head, was defined as the larva's location. The direction of the tail was found by finding the maximum pixel value on a 0.65 mm diameter circle around this point, which corresponded roughly to the position of the swim bladder. To evaluate tail curvature we successively computed the angles of seven tail segments 0.39 mm long, by finding the center of mass of the pixel values along an arc centered on the end of the previous segment. Tail curvature was measured by summing the absolute deviation from the body angle at the head at all points along the tail. This measure was used to find the start and end of individual

bouts. A custom-made script written in Matlab 2010 (Mathworks) was used to compute the kinematic parameters online. The angle of the last segment is used to count the number of oscillations of each bout and measure the tail-beat frequency as the inverse of the time between successive extreme tail positions in the same direction. The head yaw is defined as the maximum peak-to-peak amplitude of the angle of a line between the swim bladder and a point between the two eyes of the larva during each forward bout. Detected bouts with one cycle of oscillation or less were excluded.

Spinal injections

Larvae four to seven dpf were anaesthetized with 0.02% Tricaine (MS-222, Sigma) and pressure injected with either a 10% solution of calcium green dextran (10,000 MW, Invitrogen) in water or 10% solution of Texas Red dextran (3,000 MW, Invitrogen) in water into axons in the spinal cord to retrogradely label reticulospinal cell somas as described previously ((Huang et al., 2013; O'Malley et al., 1996; Orger et al., 2008). Larvae were given one or more days to recover in E3 medium following injection. All experiments requiring injection were performed on AB WT larvae homozygous for the nacre mutation (*mitfa* -/-) which reduces melanophore pigmentation throughout the skin but not eyes, making imaging more permissible without compromising visual function.

Custom built two-photon microscope with projected visual stimulus

The custom built two-photon microscope used a Mai Tai HP Ti-Sapphire laser tuned to 950 nm. The visual stimulus consisted of a square OMR grating of period 10 mm. It was projected, using an amber (590 nm) LED mounted into a miniature LCOS projector, onto an opal glass screen directly underneath the larva. Stimulus light was filtered with a narrow band-pass filter, and there was no detectable stimulus bleed-through.

Two-photon imaging of nMLF cells in paralyzed larvae

Each plane was imaged for 200 seconds at 7.23 frames per second using a quad-interlaced scan pattern that ensured that each cell was sampled evenly at four times this frame rate. The visual stimulus shown during the 200 seconds per plane consisted of 10 trials of moving gratings, each lasting 10 seconds, with 10 seconds of static gratings in between trials. The trials were always shown in the same order for ease of analysis. These stacks were analyzed using software custom written in Matlab (Mathworks). The software allows users to select the same cell in different planes and then computes the fluorescence traces for the cell (the full three-dimensional region of interest or ROI) for the full 1440 frames that includes the 10 presentations of moving gratings and the 10 periods of static gratings. The baseline fluorescence for the cell was calculated as the average fluorescence for the whole ROI across frames when the static grating was presented.

Two-photon imaging of nMLF cells in paralyzed larvae with accompanying fictive recordings of motor output

Nacre -/- AB larvae were injected with calcium green dextran as above at 5 dpf. At 7 dpf, larvae were prepared for experiments by mounting in low-melting temperature agarose, injected with 1 mM α-bungarotoxin (Tocris), and an access window was cut out of the agarose on the right side of the body from the swim bladder to the anal pore. During recordings, intact larvae were placed under 20x magnification and a recording electrode was positioned in contact with the side of the body while a gentle suction was applied. Trials consisted of 10 seconds of baseline recording, 10 seconds of grating motion, and 10 seconds following motion during imaging in a single plane at 6 Hz. Ventral root recordings were made with borosilicate glass pipettes (resistance 0.5-1 mΩ) sucked onto the muscle at the myotomal border, filled with external solution pH 7.7 (Drapeau et al., 1999). Data were acquired in current mode using Clampex 10.3.14 software

(Molecular Devices) AC 300 Hz, Gain 500, Bessel 2.2 kHz. Custom microscope and imaging software provided by Intelligent Imaging Innovations, Inc. (3i, Denver, CO) including a Mai Tai Deepsee laser (Spectra-Physics) tuned to 950 nm and a Zeiss Axio Examiner Z1 with a Zeiss W Plan-APO 20x water-immersion objective. Gratings were presented using an MP160 pocket projector (3M) filtered with a Wratten #29 (Kodak). The stimulus was created using Labview 2012 (National Instruments) and delivered as above except presentation was on the left side of the animal rather than underneath. Data were analyzed using custom software in Matlab (Mathworks, Natick, MA).

SUPPLEMENTAL FIGURE 1

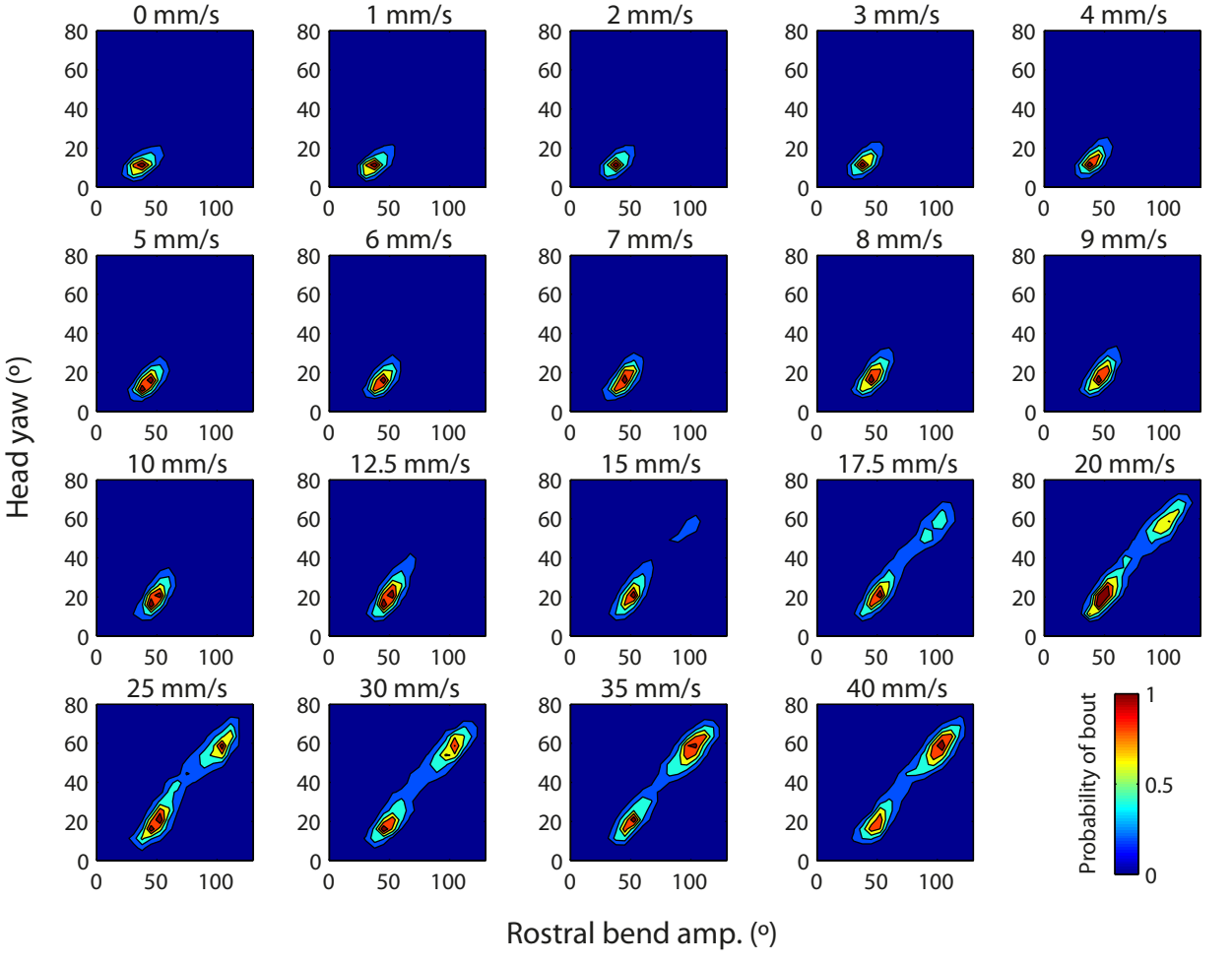

SUPPLEMENTAL FIGURE 2

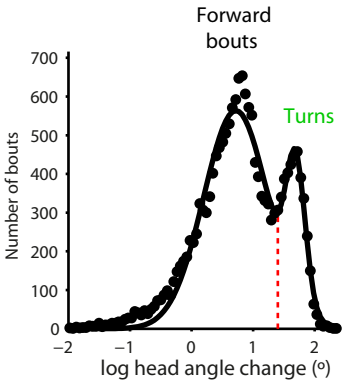

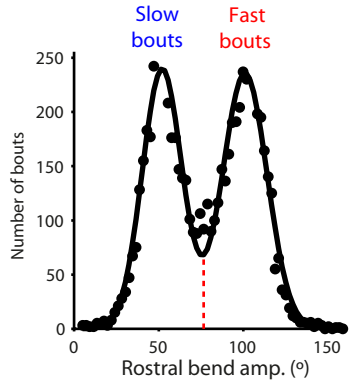

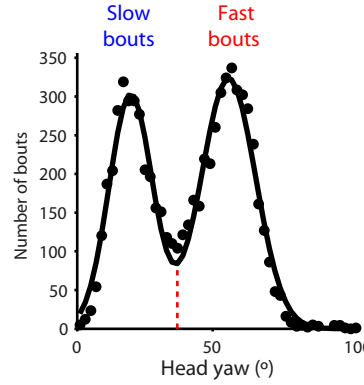

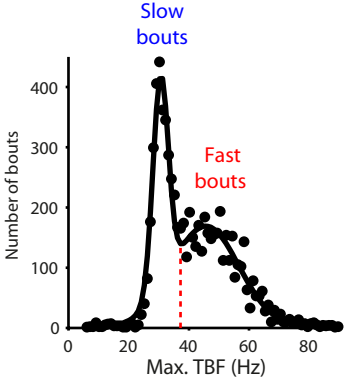

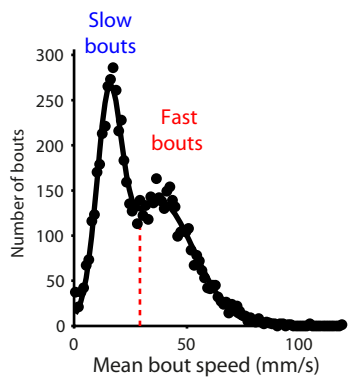

SUPPLEMENTAL FIGURE 3

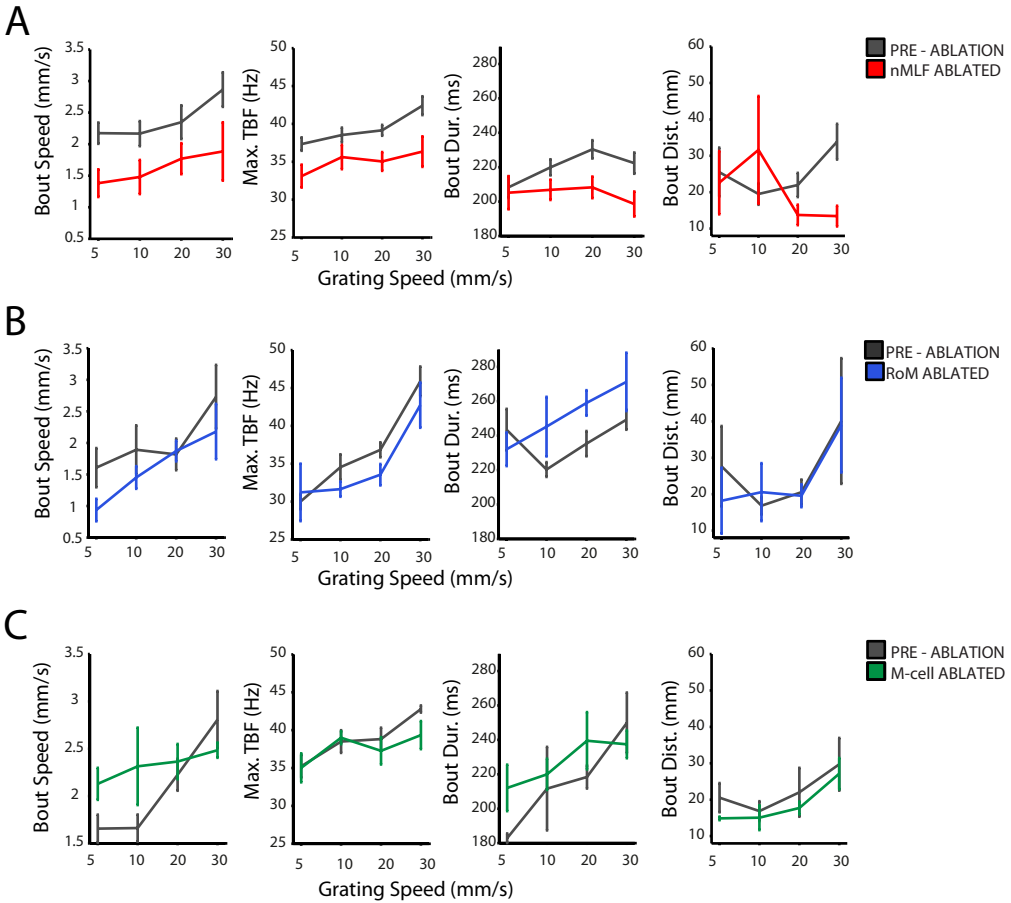

SUPPLEMENTAL FIGURE 4

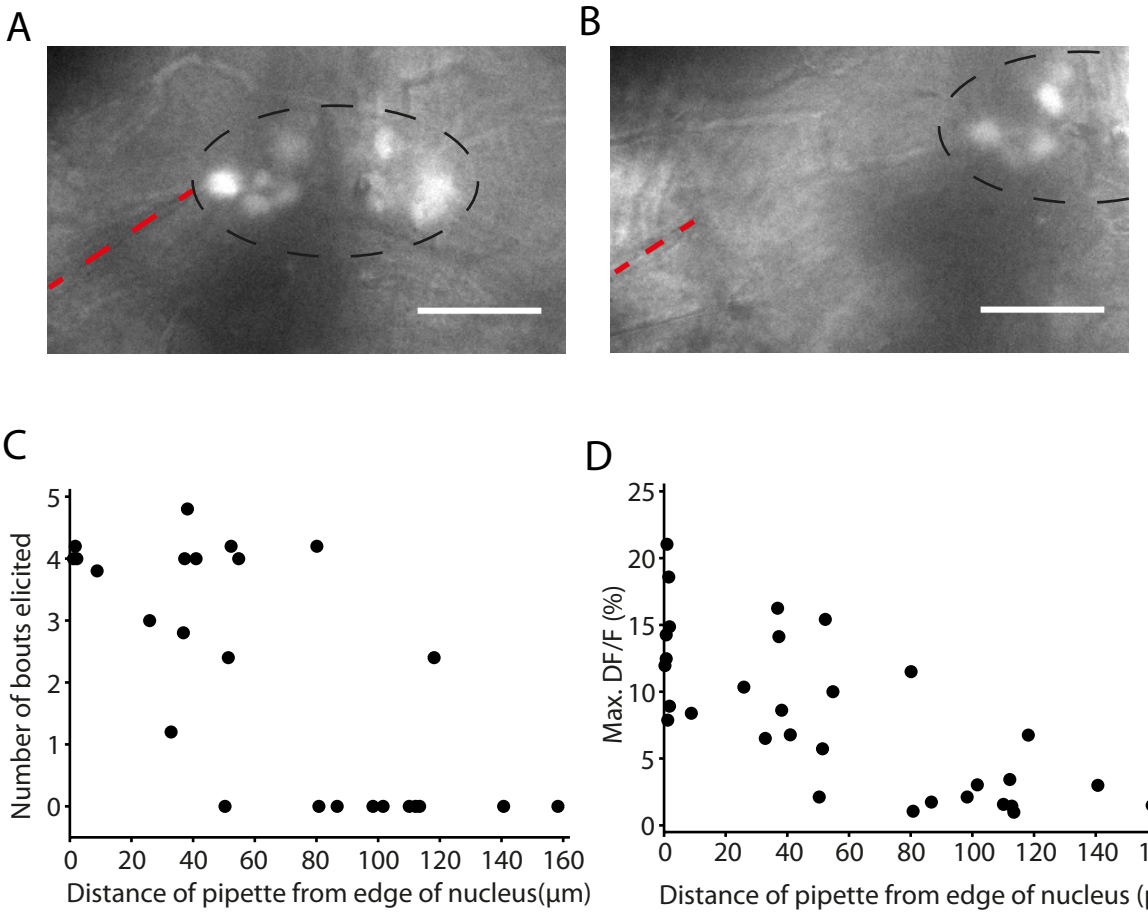

SUPPLEMENTAL FIGURE 5

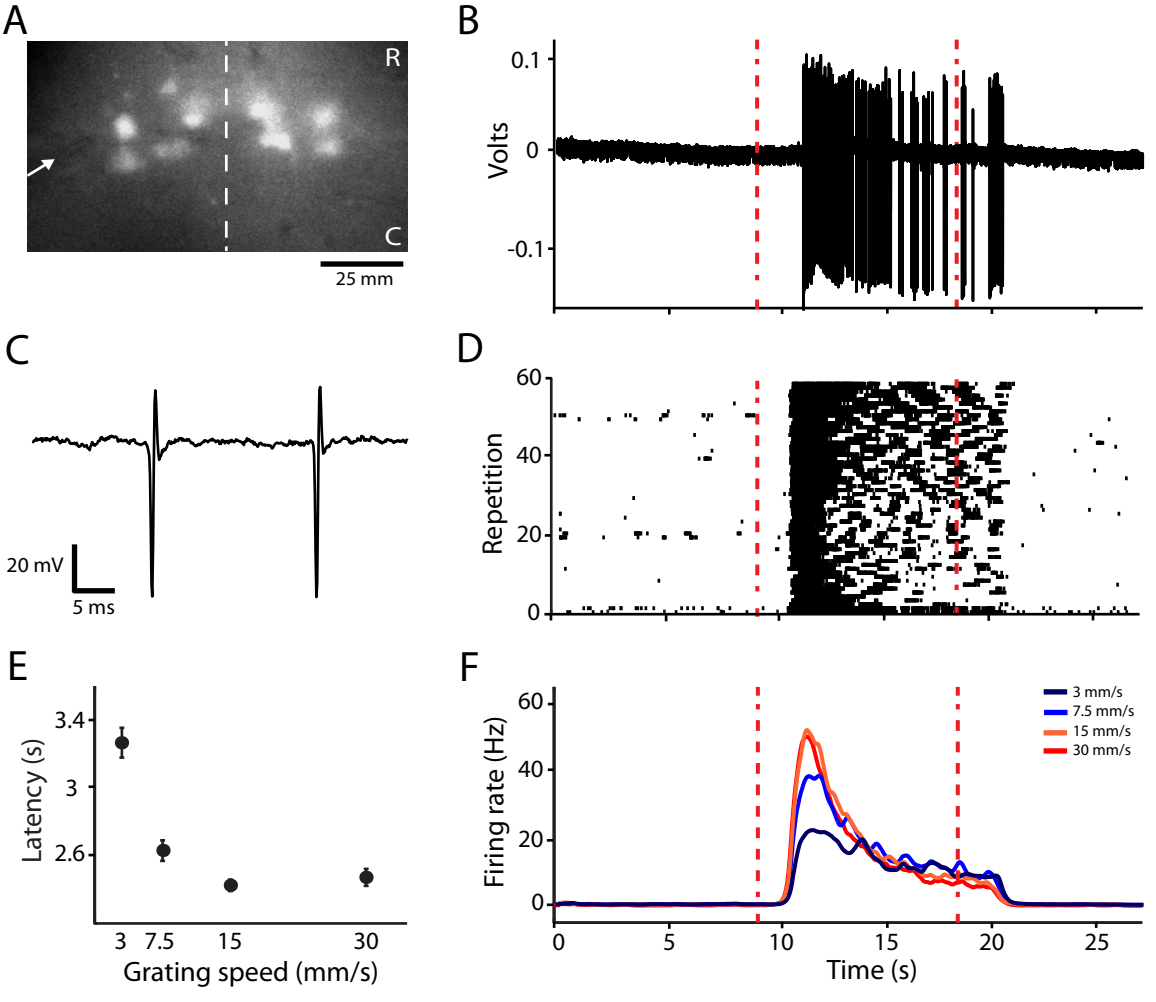

SUPPLEMENTAL FIGURE 6

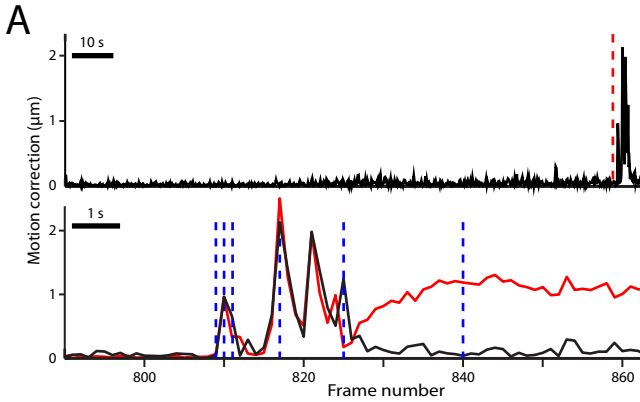

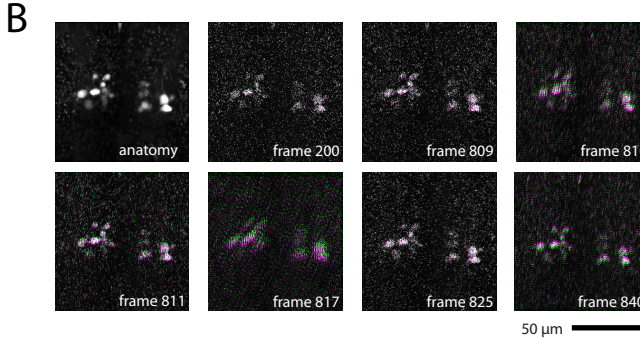

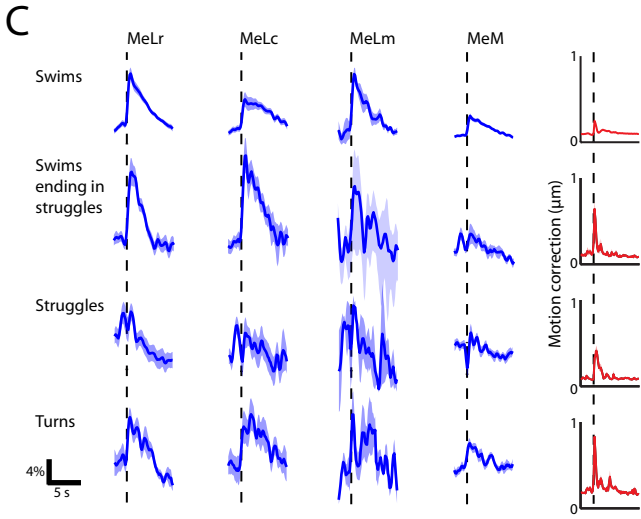

SUPPLEMENTAL FIGURE 7

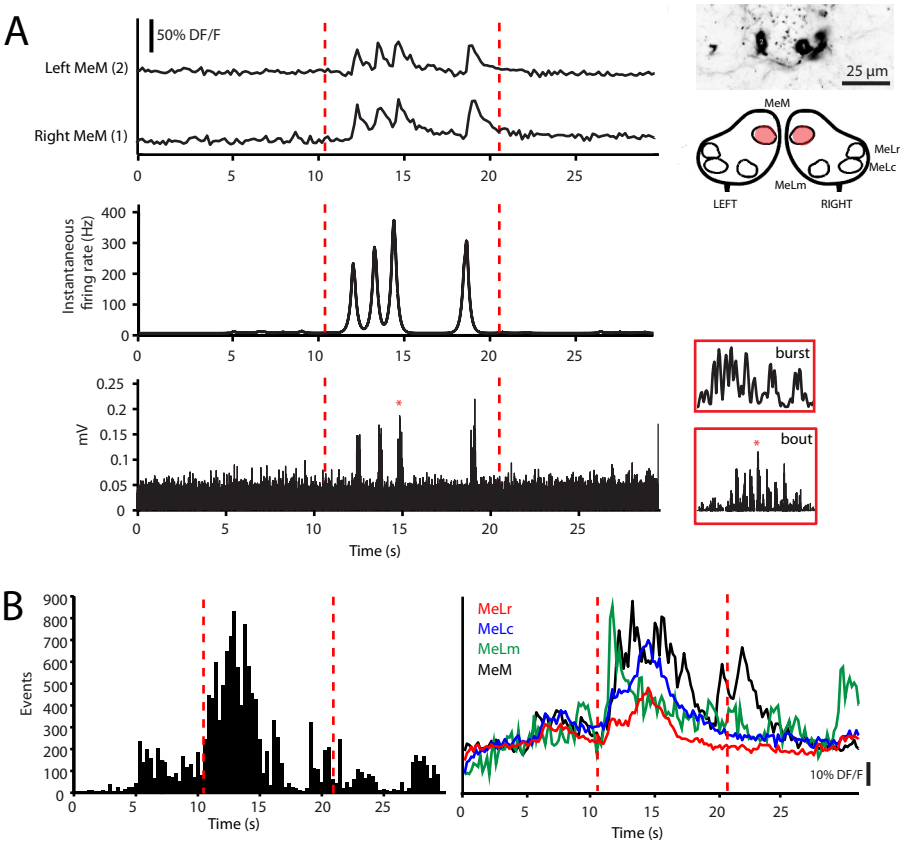

SUPPLEMENTAL FIGURE 8

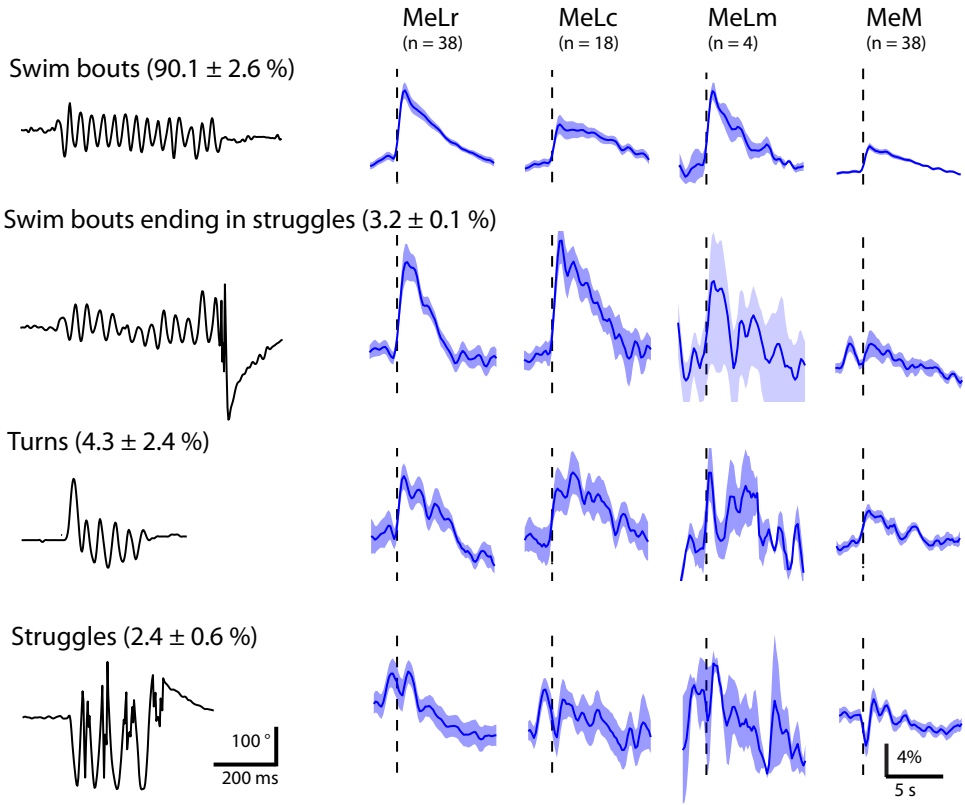

SUPPLEMENTAL FIGURE 9

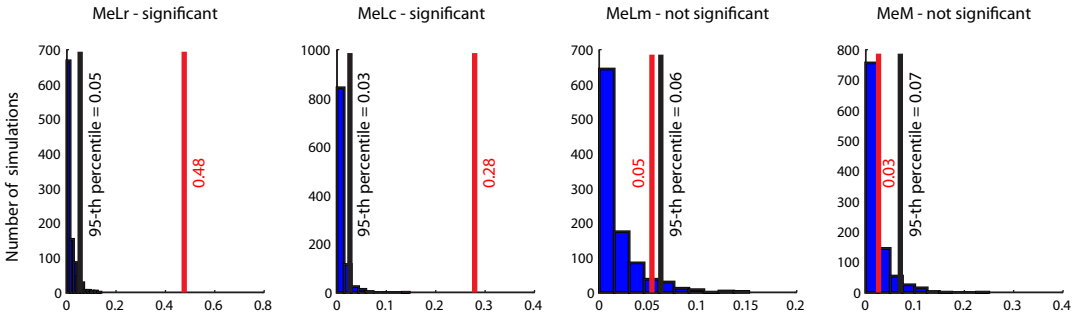

SUPPLEMENTAL FIGURE 10

A

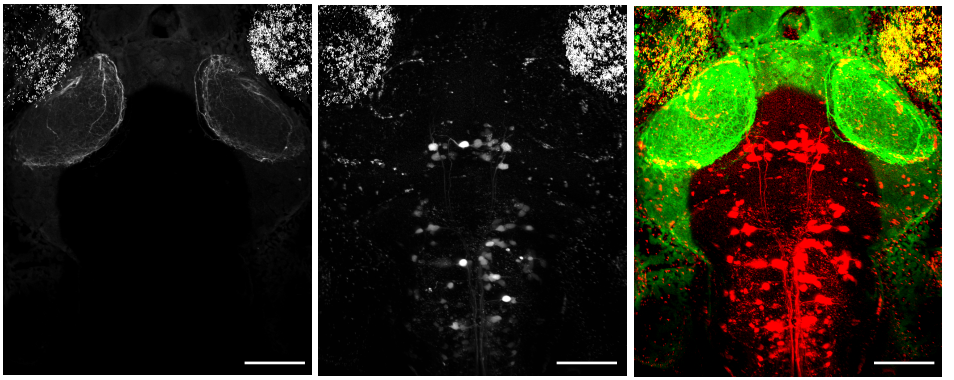

Ath5:Gal4; UAS:Dendra | Texas-Red Dextran backfill | Merge

B

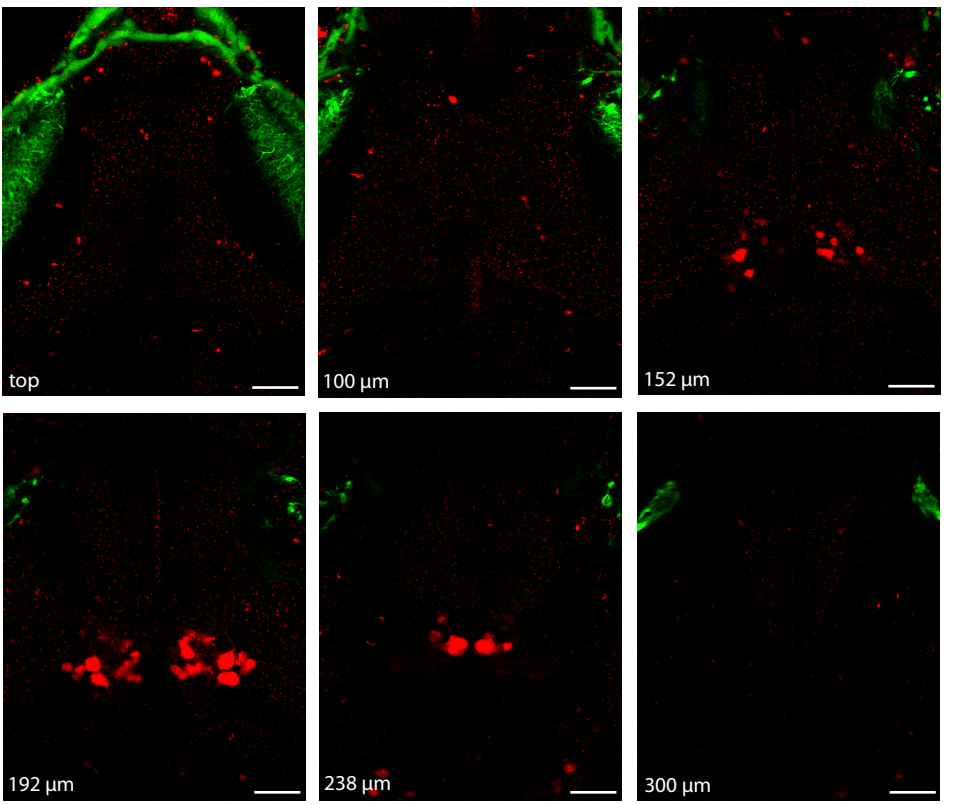

SUPPLEMENTAL FIGURE 11

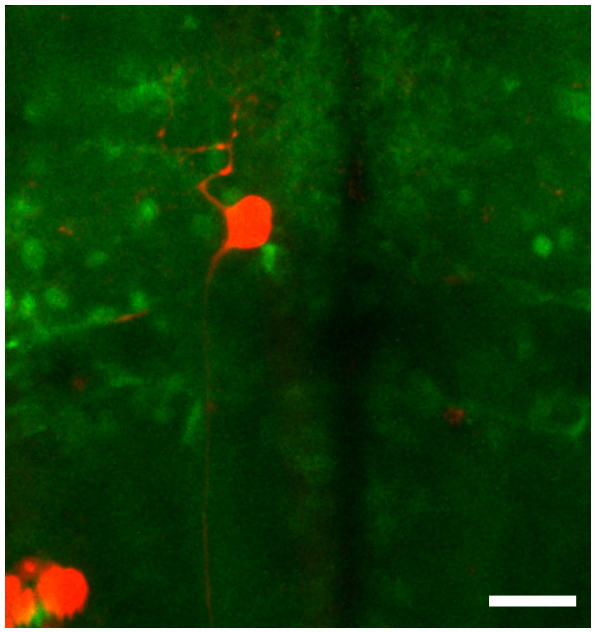

Pre-ablation
Single MeLm neuron

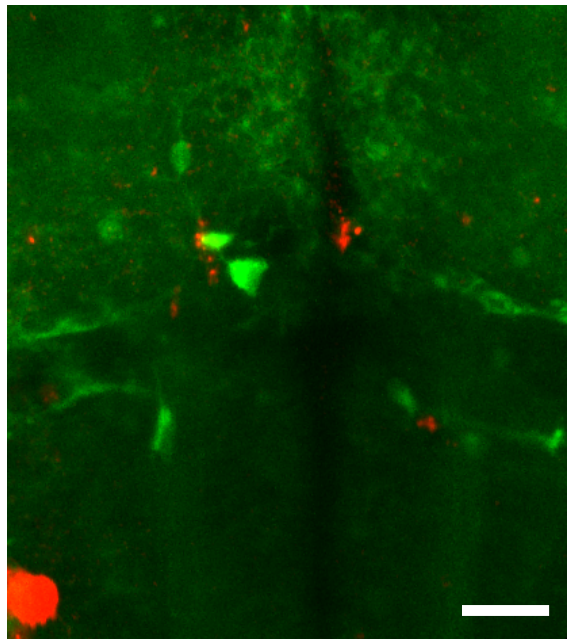

Post-ablation
Single MeLm neuron

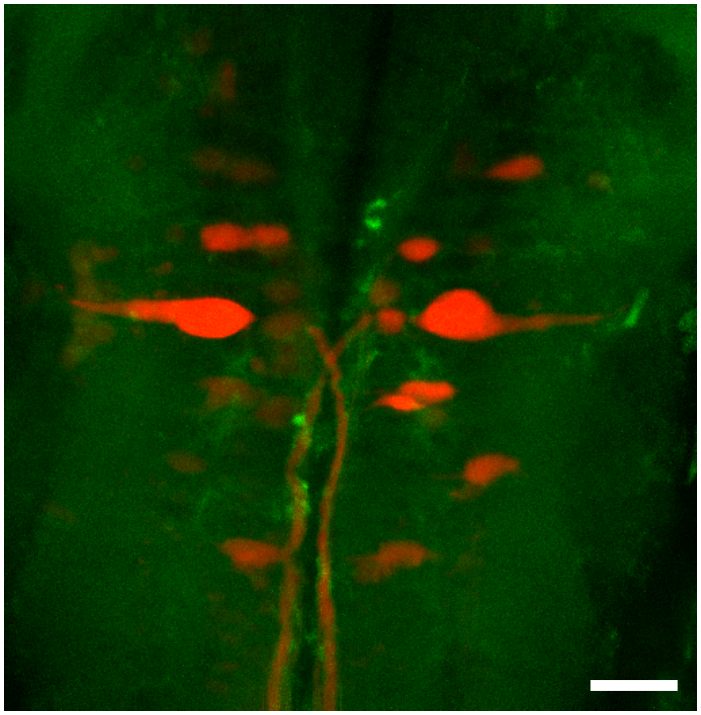

Pre-ablation
Right Mauthner Cell

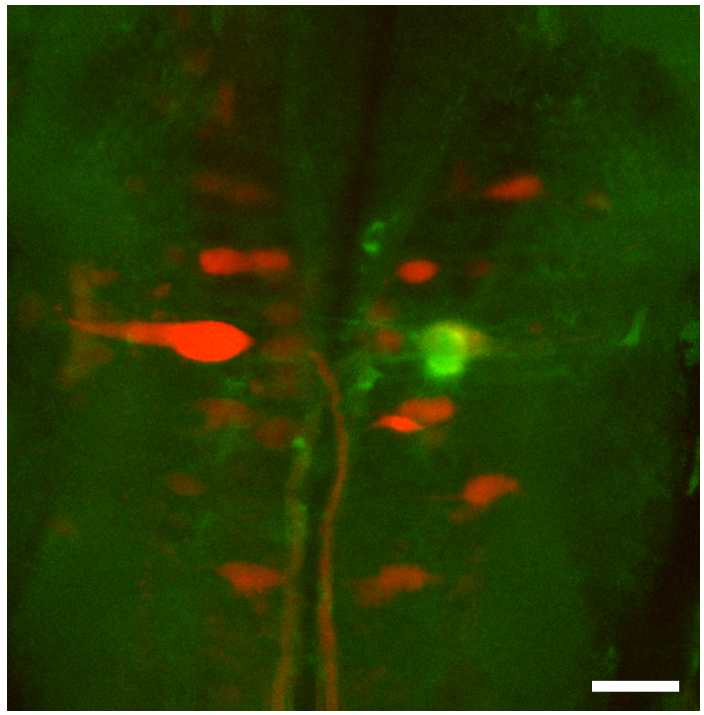

Post-ablation
Right Mauthner Cell